Wide-area Active Frequency Control with Multi-Step-Size MPC

Yan Xie, *Member*, *IEEE*, *Member*, *CSEE*, Shiying Ma, *Fellow*, *CSEE*, Jiakai Shen, *Member*, *IEEE*, *Member*, *CSEE*, Xiaojun Tang, *Member*, *IEEE*, *Member*, *CSEE*, Jianmiao Ren, *Student Member*, *IEEE*, and Liwen Zheng, *Student Member*, *IEEE*

***Abstract*—The construction of UHV AC/DC hybrid power grids and the integration of large-scale renewable energy have led to significant frequency stability issues. To enhance the frequency regulation capacity within areas and fully utilize the mutual supportive capacity among areas, active frequency control (AFC) theory has been proposed and developed based on the concept of active feed-forward control. However, existing AFC methods have limitations in computational solutions and control effects in large-scale, wide-area interconnected power systems. To address these shortcomings, this paper proposes an improved AFC method based on multi-step-size model predictive control (MSS-MPC). Through multi-step-size discretization, an improved model predictive control algorithm for AFC is derived based on the iterative solution of the multi-step-size linear quadratic regulator model, which ensures control accuracy through precise prediction and enhances the control performance through additional prediction. Based on the collaboration of two-level dispatching agencies and the consideration of differences in control objectives among areas at different stages, an improved three-stage AFC strategy is proposed, which aims to suppress additional frequency disturbances after control model switching by proposing the active-passive switching strategy. Case studies demonstrate that, compared with the existing AFC method, the proposed AFC method with the MSS-MPC algorithm has a better control effect and better computational performance.**

***Index Terms*—Active control, frequency stability, model predictive control, multi-step-size, spatial temporal distribution.**

NOMENCLATURE

A. Constant Parameters and Indexes

i	Index for the current area.
j	Index for the adjacent area.
k	Index for the current step.

B. Mathematical Symbols

Δ	Deviation from the rated value.
$\dot{A}$	The first-order derivative of A with respect to t.
$A_{[k]}$	The value of A at step k.
$A_{[k\|k]}$	The value of A at step k at the kth time.

Manuscript received August 26, 2024; revised December 31, 2024; accepted January 21, 2025. Date of online publication May 16, 2025, date of current version May 25, 2025. This work was supported by the National Natural Science Foundation of China (No. U22B20109).

Y. Xie, S. Y. Ma (corresponding author, email: msy_1969@163.com), J. K. Shen, X. J. Tang, J. M. Ren, and L. W. Zheng are with the State Key Laboratory of Power Grid Safety (China Electric Power Research Institute), Beijing 100192, China.

DOI: 10.17775/CSEEJPES.2024.06280

C. Constant Parameters and Variables

f_i, f_j	Inertia center frequencies in areas i and j.
$\Delta f_{\mathrm{a},j}$	Frequency change rate of area j.
$\Delta P_{\mathrm{L},i}$	Unbalanced power.
D_i, H_i	Area equivalent damping and inertia time constant.
$R_{\mathrm{g},i}$, $R_{\mathrm{w},i}$ $R_{\mathrm{ge},i}$, $R_{\mathrm{VFR},i}$	Speed-droop characteristics of TPUs, HPUs, TPUs and VFR resources.
$k_{1,t}$, $k_{2,t}$	Power coefficients of TPUs and HPUs.
$T_{\mathrm{g},i}, T_{\mathrm{tr},i}$	Governor time constant and reheat time constant.
$T_{\mathrm{th},i}, P_{\mathrm{th},i}$	Steam chest time constant and output power.
$K_{\mathrm{tr},i}$	High pressure turbine power fraction.
$V_{\mathrm{t},i}, V_{\mathrm{w},i}$	Valve openings of TPUs and HPUs.
$P_{\mathrm{tm},i}, P_{\mathrm{w}.i}$	Output powers of TPUs and HPUs.
$P_{\mathrm{g},i}, P_{\mathrm{VFR},i}$	Output powers of GTUs and VFR resources.
$T_{\mathrm{wg},i}, T_{\mathrm{wr},i}$	Governor transient drop and reset time constant.
$T_{\mathrm{w},i}$	Turbine time constant.
$R_{\mathrm{wp},i}, R_{\mathrm{wt},i}$	Transient drop and permanent reduction rate of turbine.
$P_{\mathrm{wt},i}$	Governor output of hydropower unit.
a_i, b_i, c_i	Valve positioner time constant.
X_i, Y_i	Leading and lagging time constants of governor.
$T_{\mathrm{CR},i}$	Combustion reaction delay time constant.
$T_{\mathrm{F},i}$	Fuel time constant
$T_{\mathrm{CD},i}$	Compressor exhaust time constant.
$X_{\mathrm{e},i}$	Valve positioner.
$V_{\mathrm{e},i}$	Governor intermediate state.
$P_{\mathrm{gR},i}$	Combustion chamber intermediate state.
$T_{\mathrm{VFR},i}$	Virtual control delay.
T_{ij}	Synchronous power coefficient between i and j.
$P_{\mathrm{T},i}, P_{\mathrm{S},i}$	Power of tie line and secondary frequency regulation.
$k_{\mathrm{tp}}, k_{\mathrm{tI}}$	Proportional and integral coefficients.
B_i	Deviation coefficient.
α_i	Conversion factors for areal base values.

D. Subscripts

TPU	Thermal power unit.
HPU	Hydropower power unit.
GTU	Gas turbine unit.
VFR	Virtual frequency response.

I. Introduction

FREQUENCY stability is becoming increasingly prominent in new-type power systems due to the construction of ultra-high voltage AC/DC hybrid power grids and large-scale renewable energy [1]–[4]. Specifically, the scale of unbalanced power in power systems gradually increases, requiring a sufficient frequency regulation capability for power systems. However, new-type power systems are becoming scarce in inertial response and frequency control resources, which significantly reduces of the system frequency regulation capability [5]–[7]. The economic and time costs of new frequency regulation resources (FRRs) from construction to usage are huge, making it impossible to quickly enhance regulation capabilities [8], [9]. Therefore, giving full play to the capabilities of existing FRRs becomes a major way to quickly enhance the stability of system frequency.

The conventional frequency control (TFC) method, which essentially falls into passive feedback control, is based on local frequency deviation. Then, the insufficiency of TFC performance is more prominent in wide-area interconnected power systems under the significant frequency spatial-temporal distribution (STD) characteristic [10], [11]. More specifically, frequency control triggered by local frequency deviations cannot fully invoke the regulation capability according to event severity, and cannot quickly respond to severe frequency events occurring in other area [12]. Aiming at the problems of the TFC method under severe frequency faults, active frequency control (AFC) theory has been proposed and developed by active feed-forward control means based on trend prediction.

The basic theory of AFC was first proposed in [13], where the control framework of "offline decision-making and online matching" is built. Frequency control has been changed from conventional proportional feedback control based on local frequency differences to feed-forward control triggered by parameters at fault locations. From the system perspective, an approach has been proposed to address the response delay issue arising from the spatiotemporal distribution of frequencies in wide-area power systems. To clarify application scenarios of AFC, the grading principle for the system frequency security level is put forward in [14] based on the approximate proportional mapping of the frequency nadir and the quasi-steady-state frequency, where the application basis for AFC is provided. To improve the efficiency of offline analysis, a method for identifying coherent generator groups based on the support vector clustering algorithm is proposed in [15], providing a way to reduce scenarios of offline analysis. The above study puts forward the concept of AFC, designs the control framework and clarifies applicable scenarios. However, the control algorithms adopted are relatively simple. Based on model predictive control (MPC), an AFC method for AC power grids is proposed in [16], involving a three-stage control algorithm that includes a descending period, an ascending period, and an active-passive switching period. However, the conventional MPC model has limitations, and the three-stage control algorithm is relatively rough. The objective function of MPC is improved in [17], [18], so that it could be used for security and economic coordination problems. On this basis, the technical and economic aspects of energy storage can be considered. Moreover, an AFC strategy for grid-connected wind farms is proposed in [19], and expands the objects of active control. However, the AFC study above is still relatively preliminary. The solution efficiency and control effect of the conventional MPC model and the three-stage control algorithm adopted still need to be improved.

The common MPC method, which includes a prediction model, rolling optimization, and feedback control, does not require high model accuracy and has good control performance [20], and has been widely applied to power system control. Based on the MPC method, an application in microgrid control is shown in [21]; the coordinated control of LCC-HVDC under capacity and frequency constraints is realized in [22]; the inertia of a hybrid power system is successfully improved in [23]; the fast frequency control service of a converter interface generator is realized in [24]. It can be seen that the common MPC method has a good effect on component control, but in large-scale power systems, the need to expand the prediction range to improve the control effect will lead to an exponential increase in the computational burden [25], [26]. In addition, the AFC method and AFC to TFC switching strategies are crucial for safe and stable system operation. The existing targets and switching strategies of the AFC method may lead to additional frequency disturbances [13], [17]. Therefore, the AFC method needs to be further improved.

The AFC method based on the MPC algorithm in large-scale power systems faces a contradiction between speed and accuracy. For those issues, the contributions of this paper are as follows: a) Considering that multi-step-size prediction can effectively reduce the calculation amount while expanding the prediction range [27], this paper proposes an AFC method with a multi-step-size MPC algorithm (AFC with MSS-MPC) to improve computational efficiency and control effect; b) In view of additional frequency disturbances that may arise from AFC and TFC switching, an improved three-stage control algorithm with a smooth control function is proposed to enhance frequency response at all stages.

This paper is organized as follows. Section II constructs a frequency control model for a multi-area interconnected power system. Section III proposes the AFC method with MSS-MPC based on a multi-step-size linear quadratic regulator (LQR) algorithm. Section IV proposes a modified three-stage control algorithm based on areal frequency control in the two-level dispatching mode. Section V verifies the effectiveness of the model and discusses its impacts on the control parameters. Finally, the conclusion and the outlook are given in Section VI.

II. Areal Frequency Control Modeling

A. Active Frequency Response Model

FRRs are becoming increasingly diverse, providing abundant means for system frequency regulation. At present, a frequency regulation system has been formed in interconnected power systems, in which conventional units such as thermal power units (TPU) and hydropower units (HPU) are used as

main resources for primary and secondary frequency regulation, and gas turbine units (GTU), wind power units, photovoltaic units, and energy storage units are used as important supplements. However, different FRRs have different response characteristics. For example, hydropower units and gas turbine units are affected by the water hammer effect and the air hammer effect, respectively, which will lead to power inverse-regulation during frequency response. Hence, there is a need for active coordination among various FRRs in control.

The quantity of FRRs in a system is enormous, and detailed one-by-one modeling can lead to an extremely complex model that is difficult to solve. Based on the idea of equivalent parameter modeling, an interconnected power system can be divided into a number of centralized control areas. Then, the resources of the same type within each control area are equivalently aggregated, and the AFC model describing the frequency dynamics of a certain area can be built, as shown in Fig. 1.

To make full use of frequency regulation capabilities in different areas under the STD characteristic, the area frequency deviation is used as the control signal to respectively control different FRRs within the area. Hydropower units also have a large capacity and an inverse-regulation property, which may reduce the participation of the HPU when the AFC method is used. To ensure system stability and make full use of the HPU, the HPU will be optimized and controlled uniformly with the TPUs. The typical parameters in Fig. 1 are shown in Appendix D.

As shown in Fig. 1, the frequency response loops of the conventional units and gas units include the governor and the turbine. The state equation and the constraints on the TPU are as follows:

$$\Delta\dot{V}_{\mathrm{t},i} = -\frac{1}{R_{\mathrm{g},i}T_{\mathrm{g},i}}u_{1,i} - \frac{1}{T_{\mathrm{g},i}}\Delta V_{\mathrm{t},i} + \frac{k_{1,i}}{T_{\mathrm{g},i}}\Delta P_{\mathrm{S},i} \tag{1a}$$

$$\Delta\dot{P}_{\mathrm{th},i} = \frac{1}{T_{\mathrm{th},i}}\Delta V_{\mathrm{t},i} - \frac{1}{T_{\mathrm{th},i}}\Delta P_{\mathrm{th},i} \tag{1b}$$

$$\Delta\dot{P}_{\mathrm{tm},i} = \frac{K_{\mathrm{tr},i}}{T_{\mathrm{th},i}}\Delta V_{\mathrm{t},i} + \frac{T_{\mathrm{th},i} - K_{\mathrm{tr},i}T_{\mathrm{tr},i}}{T_{\mathrm{tr},i}T_{\mathrm{th},i}}\Delta P_{\mathrm{th},i} - \frac{1}{T_{\mathrm{tr},i}}\Delta P_{\mathrm{tm},i} \tag{1c}$$

$$\Delta V_{\mathrm{t,min},i} \le \Delta V_{\mathrm{t},i} \le \Delta V_{\mathrm{t,max},i} \tag{1d}$$

$$\Delta P_{\mathrm{tm,min},i} \le \Delta P_{\mathrm{tm},i} \le \Delta P_{\mathrm{tm,max},i} \tag{1e}$$

And the state equation and the constraints on the HPU are as follows:

$$\Delta\dot{V}_{\mathrm{w},i} = -\frac{1}{T_{\mathrm{wg},i}R_{\mathrm{w},i}}\Delta u_{1,i} + \frac{k_{2,i}}{T_{\mathrm{wg},i}}\Delta P_{\mathrm{S},i} - \frac{1}{T_{\mathrm{wg},i}}\Delta V_{\mathrm{w},i} \tag{2a}$$

$$\Delta\dot{P}_{\mathrm{wt},i} = \frac{R_{\mathrm{wp},i}T_{\mathrm{wg},i} - R_{\mathrm{wp},i}T_{\mathrm{wr},i}}{R_{\mathrm{wt},i}T_{\mathrm{wr},i}T_{\mathrm{wg},i}}\Delta V_{\mathrm{w},i} + \frac{k_{2,i}R_{\mathrm{wp},i}}{R_{\mathrm{wt},i}T_{\mathrm{wg},i}}\Delta P_{\mathrm{S},i} - \frac{R_{\mathrm{wp},i}}{R_{\mathrm{wt},i}T_{\mathrm{wr},i}}\Delta P_{\mathrm{wt},i} - \frac{R_{\mathrm{wp},i}}{T_{\mathrm{wg},i}R_{\mathrm{w},i}R_{\mathrm{wt},i}}\Delta u_{1,i} \tag{2b}$$

$$\Delta\dot{P}_{\mathrm{w},i} = -\frac{2}{T_{\mathrm{w},i}}\Delta P_{\mathrm{w},i} + \frac{2R_{\mathrm{wt},i}T_{\mathrm{wr},i} + 2R_{\mathrm{wp},i}T_{\mathrm{w},i}}{R_{\mathrm{wt},i}T_{\mathrm{wr},i}T_{\mathrm{w},i}}\Delta P_{\mathrm{wt},i} - \frac{2R_{\mathrm{wp},i}T_{\mathrm{wg},i} - 2R_{\mathrm{wp},i}T_{\mathrm{wr},i}}{R_{\mathrm{wt},i}T_{\mathrm{wr},i}T_{\mathrm{wg},i}}\Delta V_{\mathrm{w},i} - \frac{2k_{2,i}R_{\mathrm{wp},i}}{T_{\mathrm{wg},i}R_{\mathrm{wt},i}}\Delta P_{\mathrm{S},i} + \frac{R_{\mathrm{wp},i}}{T_{\mathrm{wg},i}R_{\mathrm{w},i}R_{\mathrm{wt},i}}\Delta u_{1,i} \tag{2c}$$

$$\Delta P_{\mathrm{w,min},i} \le \Delta P_{\mathrm{w},i} \le \Delta P_{\mathrm{w,max},i} \tag{2d}$$

In the GTU, the state equation and the constraints are as follows:

$$\Delta\dot{X}_{\mathrm{e},i} = -\frac{a_i}{R_{\mathrm{e},i}b_i}\Delta u_{2,i} - \frac{c_i}{b_i}\Delta X_{\mathrm{e},i} \tag{3a}$$

$$\Delta\dot{V}_{\mathrm{e},i} = -\frac{a_iX_i}{R_{\mathrm{e},i}b_iY_i}\Delta u_{2,i} + \frac{b_i - c_iX_i}{b_iY_i}\Delta X_{\mathrm{e},i} - \frac{1}{Y_i}\Delta V_{\mathrm{e},i} \tag{3b}$$

$$\Delta\dot{P}_{\mathrm{gR},i} = \frac{Y_i - T_{\mathrm{CR},i}}{Y_iT_{\mathrm{F},i}}\Delta V_{\mathrm{e},i} - \frac{T_{\mathrm{CR},i}}{T_{\mathrm{F},i}}\frac{a_iX_i}{R_{\mathrm{e},i}b_iY_i}\Delta u_{2,i} + \frac{T_{\mathrm{CR},i}}{T_{\mathrm{F},i}}\frac{b_i - c_iX_i}{b_iY_i}\Delta X_{\mathrm{e},i} - \frac{1}{T_{\mathrm{F},i}}\Delta P_{\mathrm{gR},i} \tag{3c}$$

$$\Delta\dot{P}_{\mathrm{g},i} = \frac{1}{T_{\mathrm{CD},i}}\Delta P_{\mathrm{gR},i} - \frac{1}{T_{\mathrm{CD},i}}\Delta P_{\mathrm{g},i} \tag{3d}$$

$$\Delta P_{\mathrm{g,min},i} \le \Delta P_{\mathrm{g},i} \le \Delta P_{\mathrm{g,max},i} \tag{3e}$$

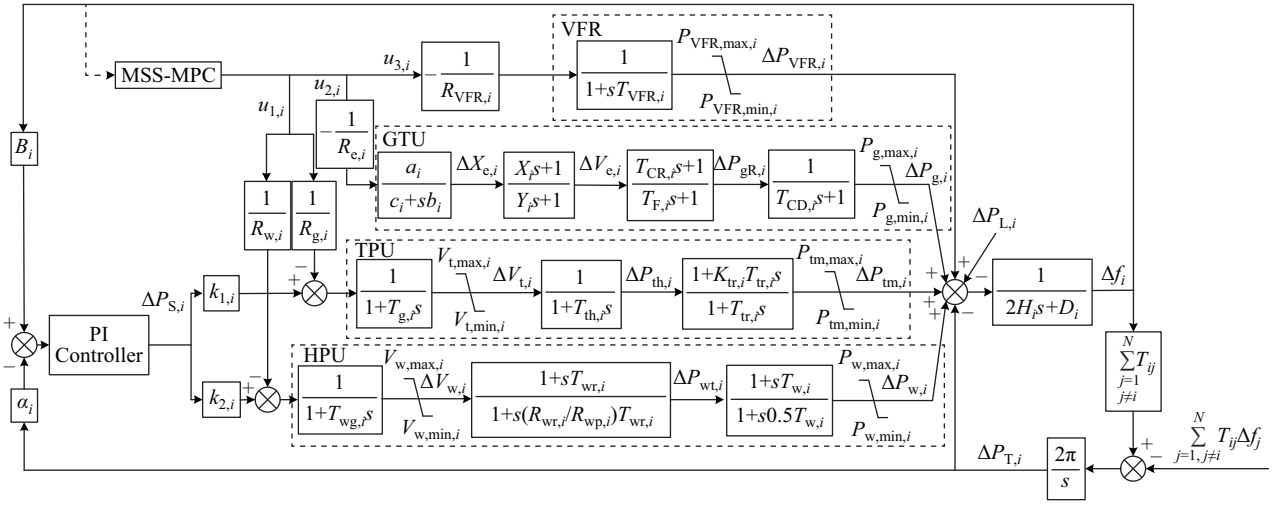

Fig. 1. Active frequency control model for area i.

With the development of new types of power systems, resources such as wind power, photovoltaic power, and energy storage that are connected to the grid through power electronic interfaces need to have frequency regulation capabilities. In fact, the frequency regulation effect of virtual frequency response (VFR) resources can be faster and more flexible than that of conventional resources, which is limited by the reserve of frequency regulation capacities. Considering the droop control and reserve restriction of resources [28], the state equation and constraint are as follows:

$$\Delta\dot{P}_{\mathrm{VFR},i} = -\frac{1}{T_{\mathrm{VFR},i}R_{\mathrm{VFR},i}}u_{3,t} - \frac{1}{T_{\mathrm{VFR},i}}\Delta\dot{P}_{\mathrm{VFR},i} \quad (4a)$$

$$\Delta P_{\mathrm{VFR,\,min},i} \le \Delta P_{\mathrm{VFR},i} \le \Delta P_{\mathrm{VFR,\,max},i} \quad (4b)$$

The state equation and the constraints of the tie-line power deviation are as follows:

$$\Delta\dot{P}_{\mathrm{T},i} = 2\pi\sum_{j=1,j\neq i}^{N} T_{\mathrm{L},ij}\Delta f_i - 2\pi\sum_{j=1,j\neq i}^{N} T_{\mathrm{L},ij}\Delta f_j \quad (5a)$$

$$\Delta P_{\mathrm{T,min},i} \le \Delta P_{\mathrm{T},i} \le \Delta P_{\mathrm{T,max},i} \quad (5b)$$

The state equation of secondary frequency modulation is:

$$\begin{aligned}\Delta\dot{P}_{\mathrm{S},i} = {} & \left(k_{\mathrm{tI}}B_i - \frac{k_{\mathrm{tP}}B_iD_i}{2H_i}\right)\Delta f_i + \frac{k_{\mathrm{tP}}B_i}{2H_i}\Delta P_{\mathrm{tm,i}} \\ & + \frac{k_{\mathrm{tP}}B_i}{2H_i}\Delta P_{\mathrm{w},i} + \frac{k_{\mathrm{tP}}B_i}{2H_i}\Delta P_{\mathrm{g},i} + \frac{k_{\mathrm{tP}}B_i}{2H_i}\Delta P_{\mathrm{VFR},i} \\ & + \left(k_{\mathrm{tI}}\alpha_{\mathrm{L},i} - \frac{k_{\mathrm{tP}}B_i}{2H_i}\right)\Delta P_{\mathrm{T},i} \\ & - k_{\mathrm{tP}}\alpha_{\mathrm{L},i}2\pi\sum_{j=1,j\neq i}^{N} T_{\mathrm{L},ij}\Delta f_j - \frac{k_{\mathrm{tP}}B_i}{2H_i}\Delta P_{\mathrm{L},i}\end{aligned} \quad (6)$$

System frequency deviations are related to the inertia, damping, unbalanced power, and power increment of each resource. Currently, power imbalance in real power systems arises mainly from permanent immense and short-term significant power loss faults. Among them, permanent large power loss faults lead to the largest amplitude of frequency drop and the most serious consequences. For permanent large power loss faults, this paper adopts step disturbance simulation, which can describe many scenarios in real power systems, such as generator outage, sudden load increase, new energy disconnection from the grid, DC blocking, and tie line disconnection. The state equation and the operation constraints of the system frequency deviation are as follows:

$$\begin{aligned}\Delta\dot{f}_i = {} & -\frac{D_i}{2H_i}\Delta f_i + \frac{1}{2H_i}\Delta P_{\mathrm{tm},i} + \frac{1}{2H_i}\Delta P_{\mathrm{w},i} + \frac{1}{2H_i}\Delta P_{\mathrm{g},i} \\ & + \frac{1}{2H_i}\Delta P_{\mathrm{VFR},i} - \frac{1}{2H_i}\Delta P_{\mathrm{T},i} - \frac{1}{2H_i}\Delta P_{\mathrm{L},i}\end{aligned} \quad (7a)$$

$$\Delta\dot{f}_j = \Delta f_{\mathrm{a},j} \quad (7b)$$

$$\Delta f_{\min,i} \le \Delta f_i \le \Delta f_{\max,i} \quad (7c)$$

It should be noted that frequency control resources in different power systems are all different in composition, which leads to the diversity of system frequency control models. For real power systems, the control resources within an area may be different from those shown in Fig. 1. For example, the area may contain virtual inertia control resources or load-side frequency regulation resources, etc., but this will not necessarily lead to the failure of the proposed AFC model. Specifically, any frequency control model that can be simplified to the form of the transfer function and linear constraints can be incorporated into the proposed AFC model. Then, the derivation can be carried out based on the method proposed in this paper.

B. State Equation Discretization

After combining the above state equations, and merging $\Delta P_{\mathrm{L},i}$ into the state variables, the standard form of the continuous state-space equation for area i can be obtained:

$$\begin{cases}\dot{\boldsymbol{x}}_i(t) = \boldsymbol{A}_i\boldsymbol{x}_i(t) + \boldsymbol{B}_i\boldsymbol{u}_i(t) \\ \boldsymbol{y}_i(t) = \boldsymbol{C}_i\boldsymbol{x}_i(t)\end{cases} \quad (8a)$$

where $\boldsymbol{A}_i$, $\boldsymbol{B}_i$ and $\boldsymbol{C}_i$ are the state matrix, control matrix and observation matrix respectively, and their specific expressions are shown in Appendix A. $\boldsymbol{x}_i(t)$, $y_i(t)$ and $\boldsymbol{u}_i(t)$ are the state variable, control variable and output variable respectively:

$$\begin{aligned}\boldsymbol{x}_i(t) = [&\Delta\boldsymbol{f}_i \;\; \Delta\boldsymbol{P}_{\mathrm{tm},i} \;\; \Delta\boldsymbol{P}_{\mathrm{th},i} \;\; \Delta\boldsymbol{V}_{\mathrm{t},i} \;\; \Delta\boldsymbol{P}_{\mathrm{w},i} \;\; \Delta\boldsymbol{P}_{\mathrm{wt},i} \\ & \Delta\boldsymbol{V}_{\mathrm{w},i} \;\; \Delta\boldsymbol{P}_{\mathrm{g},i}\Delta\boldsymbol{P}_{\mathrm{gR},i} \;\; \Delta\boldsymbol{V}_{\mathrm{e},i} \;\; \Delta\boldsymbol{X}_{\mathrm{e},i} \;\; \Delta\boldsymbol{P}_{\mathrm{VFR},i} \\ & \Delta\boldsymbol{P}_{\mathrm{T},i} \;\; \Delta\boldsymbol{P}_{\mathrm{S},i} \;\; \Delta\boldsymbol{f}_j \;\; \Delta\boldsymbol{P}_{\mathrm{L},i} \;\; \Delta\boldsymbol{f}_{\mathrm{a}}]^{\mathrm{T}}\end{aligned} \quad (8b)$$

$$\boldsymbol{u}_i(t) = [\boldsymbol{u}_{1,i}(t) \;\; \boldsymbol{u}_{2,i}(t) \;\; \boldsymbol{u}_{3,i}(t)]^{\mathrm{T}} \quad (8c)$$

In order to accommodate real discrete control systems, a multi-step improved control algorithm is adopted to achieve optimal control, where two different sampling steps, $T_{d1,i}$ and $T_{d2,i}$, are set. Based on the zero-order hold method, assuming that $u_i(t)$ remains unchanged during the sampling period, the discretized linearized equations are as follows:

$$\begin{cases}\boldsymbol{x}_{i[k+1]} = \boldsymbol{A}_{\mathrm{F},i,\tau}\boldsymbol{x}_{i[k]} + \boldsymbol{B}_{\mathrm{F},i,\tau}\boldsymbol{u}_{i[k]} \\ \boldsymbol{y}_{i[k+1]} = \boldsymbol{C}_i\boldsymbol{x}_{i[k]}\end{cases}, \tau = 1, 2 \quad (9a)$$

$$\begin{cases}\boldsymbol{A}_{\mathrm{F},i,\tau} = \mathrm{e}^{\boldsymbol{A}_iT_{\mathrm{d},i,\tau}} \\ \boldsymbol{B}_{\mathrm{G},i,\tau} = \boldsymbol{A}_i^{-1}(\boldsymbol{A}_{\mathrm{F},i,\tau} - I)\boldsymbol{B}_i\end{cases} \quad (9b)$$

where $\boldsymbol{A}_{\mathrm{F},i,\tau}$ and $\boldsymbol{B}_{\mathrm{G},i,\tau}$ are the discretized state matrix and the control matrix; τ is the step size number of MPC. This paper takes two step sizes as an example, based on which any method containing more step sizes can be derived.

The discretization results depend on the sampling step size, but a larger sampling step size leads to lower computational accuracy. Numerical problems such as model non-convergence would arise when the sampling step size exceeds a certain range. Typically, the maximum step size is closely related to the minimum time constant of the system. In this paper, the precise prediction interval and the additional prediction interval are set respectively, where the control strategy is mainly determined by the shorter step size in the precise prediction interval, and is determined secondarily by the trend prediction of the longer step size in the additional prediction interval.

The bases for the selection of the two sampling step sizes are different. The sampling step size in the precise prediction interval has to meet the control precision requirements. As for

the sampling step size in the additional prediction interval, the larger it is, the better it will be. Since the problems examined in this paper are on an electromechanical transient time scale, a sampling time of 0.01 s can usually be selected for the precise prediction interval. Since the larger the sampling time in the additional prediction interval is, the greater the error will be, its sampling time should be the maximum value within the tolerable range. This value can be selected based on numerical simulation, it can reflect the frequency change trend and cause no numerical problem.

III. MSS-MPC Algorithm for AFC Method

In order to achieve an efficient and robust AFC method, the LQR model is adopted [29]. By adding the additional prediction interval based on multi-sampling step discretization, the performance of the model predictive controller is improved. Thus, the MSS-MPC algorithm for the AFC method based on a multi-step-size LQR is proposed in this chapter.

A. Formal Transformation of Discrete State Equation

The control objective in each area is different. Therefore, the AFC method with an MPC algorithm in different areas is a comprehensive control problem involving the trajectory tracking problem (tracking a certain target trajectory) and the regulation problem (tracking the zero state value). To consider frequency variation trends of other areas in the model, a linear target state transfer matrix is introduced as follows:

$$\boldsymbol{x}_{\mathrm{d},i[k+1]} = \boldsymbol{A}_{\mathrm{D},i,\tau}\boldsymbol{x}_{\mathrm{d},i[k]},\ \tau = 1,2 \tag{10a}$$

where $\boldsymbol{x}_{\mathrm{d},i,\tau[k]}$ is the control target at point k; $\boldsymbol{A}_{\mathrm{D},i,\tau}$ is the control target state transfer equation. $\boldsymbol{A}_{\mathrm{D},i,\tau}$ is a diagonal matrix if the control target in the area is unchanged.

To increase the robustness of control and to smoothen the control variables, input incremental control is introduced as follows:

$$\boldsymbol{u}_{i[k]} = \boldsymbol{u}_{i[k-1]} + \Delta\boldsymbol{u}_{i[k]} \tag{10b}$$

Substituting (10b) into (9a) results in:

$$\boldsymbol{x}_{i[k+1]} = \boldsymbol{A}_{\mathrm{F},i,\tau}\boldsymbol{x}_{i[k]} + \boldsymbol{B}_{\mathrm{F},i,\tau}\boldsymbol{u}_{i[k-1]} + \boldsymbol{B}_{\mathrm{F},i,\tau}\Delta\boldsymbol{u}_{i[k]},\ \tau = 1,2 \tag{10c}$$

In summary, when (10a)–(10c) are combined, the extended state equation is as follows:

$$\boldsymbol{x}_{\mathrm{a},i[k+1]} = \begin{bmatrix}\boldsymbol{x}_{i[k+1]}\\ \boldsymbol{x}_{\mathrm{d},i[k+1]}\\ \boldsymbol{u}_{i[k]}\end{bmatrix} = \boldsymbol{A}_{\mathrm{aF},i,\tau}\begin{bmatrix}\boldsymbol{x}_{i[k]}\\ \boldsymbol{x}_{\mathrm{d},i[k]}\\ \boldsymbol{u}_{i,[k-1]}\end{bmatrix} + \boldsymbol{B}_{\mathrm{aG},i,\tau}\Delta\boldsymbol{u}_{i[k]} \tag{11a}$$

where,

$$\boldsymbol{A}_{\mathrm{aF},i,\tau} = \begin{bmatrix}\boldsymbol{A}_{\mathrm{F},i,\tau} & 0 & \boldsymbol{B}_{\mathrm{G},i,\tau}\\ 0 & \boldsymbol{A}_{\mathrm{D},i,\tau} & 0\\ 0 & 0 & \boldsymbol{I}\end{bmatrix}, \boldsymbol{B}_{\mathrm{aG},i,\tau} = \begin{bmatrix}\boldsymbol{B}_{\mathrm{G},i,\tau}\\ 0\\ \boldsymbol{I}\end{bmatrix} \tag{11b}$$

where $\boldsymbol{I}$ is the unit diagonal matrix.

Considering frequency dynamic trajectory tracking based on (11), the control target error is introduced to convert the tracking problem into the regulation problem. Based on the derived extended state equation, the error equation can be written as follows:

$$\begin{aligned}\boldsymbol{e}_{i[k]} &= \boldsymbol{x}_{i[k]} - \boldsymbol{x}_{\mathrm{d},i[k]}\\ &= [\boldsymbol{I}\quad -\boldsymbol{I}\quad 0]\begin{bmatrix}\boldsymbol{x}_{i[k+1]}\\ \boldsymbol{x}_{\mathrm{d},i[k+1]}\\ \boldsymbol{u}_{i[k]}\end{bmatrix} = \boldsymbol{C}_{\mathrm{a}}\boldsymbol{X}_{\mathrm{a},i[k]}\end{aligned} \tag{12}$$

B. Cost Function Construction

The state equation is derived as the error form of the extended state equation, from which a cost function is constructed to take into account the effects of both the precise and additional prediction intervals. With the goal of minimizing the control error and the control cost [30], the linear-quadratic regulator cost function based on the extended state variables and errors is constructed as follows:

$$\begin{aligned}J =\ & \frac{1}{2}\boldsymbol{x}_{\mathrm{a},i[k+N_1]}^{\mathrm{T}}\boldsymbol{S}_{\mathrm{a},i,1}\boldsymbol{x}_{\mathrm{a},i[k+N_1]} + \frac{1}{2}\Delta\boldsymbol{u}_{i[k+N_1]}^{\mathrm{T}}\boldsymbol{R}_{i,1}\Delta\boldsymbol{u}_{i[k+N_1]} +\\ & \frac{1}{2}\boldsymbol{x}_{\mathrm{a},i[k+NS]}^{\mathrm{T}}\boldsymbol{S}_{\mathrm{a},i,2}\boldsymbol{x}_{\mathrm{a},i[k+NS]} +\\ & \frac{1}{2}\sum_{l=0}^{N_1-1}[\boldsymbol{x}_{\mathrm{a},i[k+l]}^{\mathrm{T}}\boldsymbol{Q}_{\mathrm{a},i,1}\boldsymbol{x}_{\mathrm{a},i[k+l]} + \Delta\boldsymbol{u}_{i[k+l]}^{\mathrm{T}}\boldsymbol{R}_{i,1}\Delta\boldsymbol{u}_{i[k+l]}] +\\ & \frac{1}{2}\sum_{l=N_1+1}^{NS-1}[\boldsymbol{x}_{\mathrm{a},i[k+l]}^{\mathrm{T}}\boldsymbol{Q}_{\mathrm{a},i,2}x_{\mathrm{a},i[k+l]} + \Delta\boldsymbol{u}_{i[k+l]}^{\mathrm{T}}\boldsymbol{R}_{i,2}\Delta\boldsymbol{u}_{i,[k+l]}]\end{aligned} \tag{13a}$$

$$\begin{cases}\boldsymbol{S}_{\mathrm{a},i,\tau} = \boldsymbol{C}_{\mathrm{a}}^{\mathrm{T}}\boldsymbol{S}_{i,\tau}\boldsymbol{C}_{\mathrm{a}}\\ \boldsymbol{Q}_{\mathrm{a},i,\tau} = \boldsymbol{C}_{\mathrm{a}}^{\mathrm{T}}\boldsymbol{Q}_{i,\tau}\boldsymbol{C}_{\mathrm{a}}\end{cases},\ \tau = 1,2 \tag{13b}$$

where: J is the quadratic cost function, $\boldsymbol{R}_{i,\tau}$ is the cost matrix of control variables, $\boldsymbol{S}_{i,\tau}$ is the end cost matrix, $\boldsymbol{Q}_{i,\tau}$ is the operation cost matrix, N_1 is the sampling frequency in the precise prediction interval, N_2 is the sampling frequency in the additional prediction interval, and NS is the total sampling frequency. Let $\boldsymbol{\chi} = \{\boldsymbol{R}, \boldsymbol{S}, \boldsymbol{Q}\}$ and $\kappa = \{r, s, q\}$, and then:

$$\boldsymbol{\chi}_{i,\tau} = \mathrm{diag}(\boldsymbol{\kappa}_{i,\tau,1}\quad \boldsymbol{\kappa}_{i,\tau,2}\quad \cdots\quad \boldsymbol{\kappa}_{i,\tau,N_\tau}), \tau = 1,2 \tag{13c}$$

C. Cost Function Standardization

It can be concluded from (13) that the cost function contains the state and control variables, which result in high dimensions and complexity. To enhance the efficiency of the optimization solution and to take into account both the system state and control constraints, a standard quadratic cost function expressed in terms of control variables is derived, so that a well-established QP solver can be used to solve the optimization problem.

Based on mathematical induction, the compact form of the state equation of the precise and additional prediction intervals is derived (as shown in Appendix B) as follows:

$$\boldsymbol{X}_{\mathrm{a},i[k]} = \boldsymbol{\Phi}_i x_{\mathrm{a},i[k|k]} + \boldsymbol{\Gamma}_i\boldsymbol{U}_{i[k]} \tag{14a}$$

where,

$$\boldsymbol{X}_{\mathrm{a},i[k]} = \begin{bmatrix}\boldsymbol{X}_{\mathrm{a},i,1[k]}\\ \boldsymbol{X}_{\mathrm{a},i,2[k]}\end{bmatrix}\boldsymbol{U}_{i[k]} = \begin{bmatrix}\boldsymbol{U}_{i,1[k]}\\ \boldsymbol{U}_{i,2[k]}\end{bmatrix}$$

$$\boldsymbol{\Phi}_i = \begin{bmatrix} \boldsymbol{\Phi}_{i,1} \\ \boldsymbol{\Phi}_{i,2} \end{bmatrix} \boldsymbol{\Gamma}_i = \begin{bmatrix} \boldsymbol{\Gamma}_{i,11} & 0 \\ \boldsymbol{\Gamma}_{i,21} & \boldsymbol{\Gamma}_{i,22} \end{bmatrix} \tag{14b}$$

and where,

$$\boldsymbol{X}_{\mathrm{a},i,1[k]} = \begin{bmatrix} \boldsymbol{x}_{\mathrm{a},i[k+1|k]} \\ \boldsymbol{x}_{\mathrm{a},i[k+2|k]} \\ \cdots \\ \boldsymbol{x}_{\mathrm{a},i[k+N_1|k]} \end{bmatrix}, \ \boldsymbol{X}_{\mathrm{a},i,2[k]} = \begin{bmatrix} \boldsymbol{x}_{\mathrm{a},i[k+N_1+1|k]} \\ \boldsymbol{x}_{\mathrm{a},i[k+N_1+2|k]} \\ \cdots \\ \boldsymbol{x}_{\mathrm{a},i[k+NS|k]} \end{bmatrix}$$

$$\boldsymbol{\Phi}_{i,1} = \begin{bmatrix} \boldsymbol{A}_{\mathrm{aF},i,1} \\ \boldsymbol{A}^2_{\mathrm{aF},i,1} \\ \cdots \\ \boldsymbol{A}^{N_1}_{\mathrm{aF},i,1} \end{bmatrix} \tag{14c}$$

$$\boldsymbol{U}_{i,2[k]} = \begin{bmatrix} \boldsymbol{u}_{i[k+N_1|k]} \\ \boldsymbol{u}_{i[k+N_1+1|k]} \\ \cdots \\ \boldsymbol{u}_{i[k+NS-1|k]} \end{bmatrix}, \ \boldsymbol{U}_{i,2[k]} = \begin{bmatrix} \boldsymbol{u}_{i[k+N_1|k]} \\ \boldsymbol{u}_{i[k+N_1+1|k]} \\ \cdots \\ \boldsymbol{u}_{i[k+NS-1|k]} \end{bmatrix}$$

$$\boldsymbol{\Phi}_{12} = \begin{bmatrix} \boldsymbol{A}_{\mathrm{aF},i,2}\boldsymbol{A}^{N_1}_{\mathrm{aF},i,1} \\ \boldsymbol{A}^2_{\mathrm{aF},i,2}\boldsymbol{A}^{N_1}_{\mathrm{aF},i,1} \\ \cdots \\ \boldsymbol{A}^{N_2}_{\mathrm{aF},i,2}\boldsymbol{A}^{N_1}_{\mathrm{aF},i,1} \end{bmatrix} \tag{14d}$$

$$\boldsymbol{\Gamma}_{11} = \begin{bmatrix} \boldsymbol{B}_{\mathrm{aG},i,1} & & & \\ \boldsymbol{A}_{\mathrm{aF},i,2}\boldsymbol{B}_{\mathrm{aG},i,1} & \boldsymbol{B}_{\mathrm{aG},i,1} & & \\ \vdots & \vdots & \ddots & \\ \boldsymbol{A}^{N_1-1}_{\mathrm{aF},i,1}\boldsymbol{B}_{\mathrm{aG},i,1} & \boldsymbol{A}^{N_1-2}_{\mathrm{aF},i,1}\boldsymbol{B}_{\mathrm{aG},i,1} & \cdots & \boldsymbol{B}_{\mathrm{aG},i,1} \end{bmatrix} \tag{14e}$$

$$\boldsymbol{\Gamma}_{22} = \begin{bmatrix} \boldsymbol{B}_{\mathrm{aG},i,2} & & & \\ \boldsymbol{A}_{\mathrm{aF},i,2}\boldsymbol{B}_{\mathrm{aG},i,2} & \boldsymbol{B}_{\mathrm{aG},i,2} & & \\ \vdots & \vdots & \ddots & \\ \boldsymbol{A}^{N_2-1}_{\mathrm{aF},i,2}\boldsymbol{B}_{\mathrm{aG},i,2} & \boldsymbol{A}^{N_2-2}_{\mathrm{aF},i,2}\boldsymbol{B}_{\mathrm{aG},i,2} & \cdots & \boldsymbol{B}_{\mathrm{aG},i,2} \end{bmatrix} \tag{14f}$$

$$\boldsymbol{\Gamma}_{21} = \begin{bmatrix} \boldsymbol{A}_{\mathrm{aF},i,2}\boldsymbol{A}^{N_1-1}_{\mathrm{aF},i,1}\boldsymbol{B}_{\mathrm{aG},i,1} & \boldsymbol{A}_{\mathrm{aF},i,2}\boldsymbol{A}^{N_1-2}_{\mathrm{aF},i,1}\boldsymbol{B}_{\mathrm{aG},i,1} & \cdots & \boldsymbol{A}_{\mathrm{aF},i,2}\boldsymbol{B}_{\mathrm{aG},i,1} \\ \boldsymbol{A}^2_{\mathrm{aF},i,2}\boldsymbol{A}^{N_1-1}_{\mathrm{aF},i,1}\boldsymbol{B}_{\mathrm{aG},i,1} & \boldsymbol{A}^2_{\mathrm{aF},i,2}\boldsymbol{A}^{N_1-2}_{\mathrm{aF},i,1}\boldsymbol{B}_{\mathrm{aG},i,1} & \cdots & \boldsymbol{A}^2_{\mathrm{aF},i,2}\boldsymbol{B}_{\mathrm{aG},i,1} \\ \vdots & \vdots & \ddots & \vdots \\ \boldsymbol{A}^{N_2}_{\mathrm{aF},i,2}\boldsymbol{A}^{N_1-1}_{\mathrm{aF},i,1}\boldsymbol{B}_{\mathrm{aG},i,1} & \boldsymbol{A}^{N_2}_{\mathrm{aF},i,2}\boldsymbol{A}^{N_1-2}_{\mathrm{aF},i,1}\boldsymbol{B}_{\mathrm{aG},i,1} & \cdots & \boldsymbol{A}^{N_2}_{\mathrm{aF},i,2}\boldsymbol{B}_{\mathrm{aG},i,1} \end{bmatrix} \tag{14g}$$

It can be observed that the equation is related to the input sequence of the initial state, the precise prediction interval and the additional prediction interval. Since the initial state is known, the objective of the optimization solution is to obtain the optimal control sequence. Based on the expressions of $\boldsymbol{X}_{a,i[k]}$ and $\boldsymbol{U}_{i[k]}$, the cost function can be derived as follows:

$$J = \frac{1}{2}\boldsymbol{x}^{\mathrm{T}}_{\mathrm{a},i[k|k]}\boldsymbol{Q}_{\mathrm{a},i}\boldsymbol{x}_{\mathrm{a},i[k|k]} + \frac{1}{2}\boldsymbol{X}^{\mathrm{T}}_{i[k]}\boldsymbol{\Omega}_i\boldsymbol{X}_{i[k]} + \frac{1}{2}\boldsymbol{U}^{\mathrm{T}}_{i[k]}\boldsymbol{\Psi}_i\boldsymbol{U}_{i[k]} \tag{15a}$$

where,

$$\boldsymbol{\Omega}_i = \mathrm{diag}(\boldsymbol{Q}_{\mathrm{a},i,1}, \cdots \boldsymbol{Q}_{\mathrm{a},i,1}, \boldsymbol{S}_{\mathrm{a},i,1}, \boldsymbol{Q}_{\mathrm{a},i,2} \cdots \boldsymbol{Q}_{\mathrm{a},i,2}, \boldsymbol{S}_{\mathrm{a},i,2}) \tag{15b}$$

$$\boldsymbol{\Psi}_i = \mathrm{diag}(\boldsymbol{R}_{i,1}, \cdots \boldsymbol{R}_{i,1}, \boldsymbol{R}_{i,1}, \boldsymbol{R}_{i,2} \cdots \boldsymbol{R}_{i,2}, \boldsymbol{R}_{i,2}) \tag{15c}$$

After (14a) is substituted into (15a), and the constant term $0.5\boldsymbol{x}^{\mathrm{T}}_{\mathrm{a},i[k|k]}(\boldsymbol{Q}_{\mathrm{a},i} + \boldsymbol{\Phi}^{\mathrm{T}}_i\boldsymbol{\Omega}_i\boldsymbol{\Phi}_i)\boldsymbol{x}_{\mathrm{a},i[k|k]}$ is ignored, the standard form of the quadratic cost function is as follows:

$$\min J = \boldsymbol{U}^{\mathrm{T}}_{i[k]}\boldsymbol{F}_i x_{\mathrm{a},i[k|k]} + \frac{1}{2}\boldsymbol{U}^{\mathrm{T}}_{i[k]}\boldsymbol{H}_i\boldsymbol{U}_{i[k]} \tag{16a}$$

where $\boldsymbol{F}_{\mathrm{J},i}$ and $\boldsymbol{H}_{\mathrm{J},i}$ are the coefficient matrices of the primary and quadratic terms, respectively:

$$\begin{cases} \boldsymbol{F}_i = \boldsymbol{\Gamma}^{\mathrm{T}}_i\boldsymbol{\Omega}_i\boldsymbol{\Phi}_i \\ \boldsymbol{H}_i = \boldsymbol{\Gamma}^{\mathrm{T}}_i\boldsymbol{\Omega}_i\boldsymbol{\Gamma}_i + \boldsymbol{\Psi}_i \end{cases} \tag{16b}$$

D. Constraint Condition Standardization

Consider the constraints based on the standard LQR form shown in (16), and let the constraint be:

$$\begin{cases} \boldsymbol{M}_{i[k+l]}\boldsymbol{x}_{\mathrm{a},i[k+l]} + \boldsymbol{W}_{i[k+l]}\Delta\boldsymbol{u}_{i[k+l]} \le \boldsymbol{\beta}_{i[k+l]}, \\ \quad l = 0, \cdots NS-1 \\ \boldsymbol{M}_{i[k+l]}\boldsymbol{x}_{\mathrm{a},i[k+l]} \le \boldsymbol{\beta}_{i[k+l]}, l = NS \end{cases} \tag{17a}$$

where $\boldsymbol{M}_{i[k+l]}$ and $\boldsymbol{W}_{i[k+l]}$ are the constraint coefficient matrices of the state and control variables, respectively; $\boldsymbol{\beta}_{i[k+l]}$ is the constraint vector, where,

$$\boldsymbol{M}_{i[k+l]} = \begin{bmatrix} 0 \\ 0 \\ -\boldsymbol{I} \\ \boldsymbol{I} \end{bmatrix} \boldsymbol{W}_{i[k+l]} = \begin{bmatrix} -\boldsymbol{I} \\ \boldsymbol{I} \\ 0 \\ 0 \end{bmatrix} \boldsymbol{\beta}_{i[k+l]} = \begin{bmatrix} -\boldsymbol{u}_{\mathrm{low}} \\ \boldsymbol{u}_{\mathrm{high}} \\ -\boldsymbol{x}_{\mathrm{a,upper}} \\ \boldsymbol{x}_{\mathrm{a,upper}} \end{bmatrix} \tag{17b}$$

$$\boldsymbol{M}_{i[k+NS]} = \begin{bmatrix} -\boldsymbol{I} \\ \boldsymbol{I} \end{bmatrix} \boldsymbol{\beta}_{i[k+NS]} = \begin{bmatrix} -\boldsymbol{x}_{\mathrm{alow}} \\ \boldsymbol{x}_{\mathrm{ahigh}} \end{bmatrix} \tag{17c}$$

where $\boldsymbol{x}_{\mathrm{a,lower}}$, $\boldsymbol{x}_{\mathrm{a,upper}}$, $\boldsymbol{u}_{\mathrm{lower}}$, and $\boldsymbol{u}_{\mathrm{upper}}$ are the upper and lower constraints for the state and control variables, respectively.

Based on mathematical induction, the compact form of the constraints is derived (as shown in Appendix C) as follows:

$$\bar{\boldsymbol{M}}_{i[k]}\boldsymbol{x}_{\mathrm{a},i[k|k]} + \hat{\boldsymbol{M}}_{i[k]}\boldsymbol{X}_{i[k]} + \hat{\boldsymbol{F}}\boldsymbol{U}_{i[k]} \le \bar{\boldsymbol{\beta}}_i \tag{18a}$$

where

$$\bar{\boldsymbol{M}}_{i[k]} = \begin{bmatrix} \boldsymbol{M}_{i[k]} \\ 0 \\ 0 \\ 0 \end{bmatrix}, \ \bar{\boldsymbol{\beta}}_i = \begin{bmatrix} \boldsymbol{\beta}_{i[k]} \\ \boldsymbol{\beta}_{i[k+1]} \\ \cdots \\ \boldsymbol{\beta}_{i[k+NS]} \end{bmatrix}$$

$$\hat{\boldsymbol{F}}_i = \begin{bmatrix} \boldsymbol{W}_{i[k]} & 0 & \cdots & 0 \\ 0 & \boldsymbol{W}_{i[k+1]} & 0 & 0 \\ 0 & 0 & \ddots & 0 \\ 0 & 0 & 0 & \boldsymbol{W}_{i[k+NS-1]} \\ 0 & 0 & \cdots & 0 \end{bmatrix} \tag{18b}$$

$$\hat{\boldsymbol{M}}_{i[k]} = \begin{bmatrix} 0 & 0 & \cdots & 0 \\ \boldsymbol{M}_{i[k+1]} & 0 & 0 & 0 \\ 0 & \boldsymbol{M}_{i[k+2]} & 0 & 0 \\ 0 & 0 & \ddots & 0 \\ 0 & \cdots & 0 & \boldsymbol{M}_{i[k+NS]} \end{bmatrix} \tag{18c}$$

After (14a) is substituted into (18a), the standard form of the quadratic cost function is as follows:

$$\boldsymbol{M}_{\mathrm{eq},i}\boldsymbol{U}_{i[k]} \le \bar{\boldsymbol{\beta}}_i + \boldsymbol{b}_i\boldsymbol{x}_{\mathrm{a},i[k|k]} \tag{19a}$$

where,

$$\begin{cases} \boldsymbol{M}_{\mathrm{eq},i} = \hat{\boldsymbol{M}}_{i[k]}\boldsymbol{\Gamma}_i + \hat{\boldsymbol{F}}_i \\ \boldsymbol{b}_i = -(\bar{\boldsymbol{M}}_{i[k]} + \hat{\boldsymbol{M}}_{i[k]}\boldsymbol{\Phi}_i) \end{cases} \tag{19b}$$

The standard LQR optimization problem with constraints considering multi-step-size prediction can be obtained by combining (16) with (19). Based on the stepwise iterative solution of the multi-step-size LQR algorithm based on the QP solver, the MSS-MPC algorithm can be obtained.

IV. Multi-stage AFC Method

The AFC method is a specific means to deal with emergency scenarios, and three issues should be considered:

1) Frequency Control Objective

Due to the STD characteristic of interconnected power systems, disturbed and undisturbed areas have different frequency response delays, leading to different frequency dynamics. Therefore, different frequency control objectives should be set in different areas in a multi-area AFC system.

2) Tie-line Constraint

There is a predetermined power exchange plan for tie-lines between different areas, and each dispatching agency is responsible for its own frequency regulation. Therefore, the original exchange scheme should be resumed as soon as possible with necessary inter-area support.

3) Control Switching Strategy

With the application of the AFC method, the frequency drop rate is suppressed. However, the AFC method should be switched to the TFC method to restore the frequency regulation capacity after the emergency period. Therefore, the control switching strategy from AFC to TFC should be considered.

In summary, the multi-stage AFC method with MSS-MPC is shown in Fig. 2. Based on the disturbed and undisturbed area control architecture, the multi-stage AFC method with MSS-MPC is coordinated by the superior and areal dispatching agencies. The areal dispatching agency is responsible for developing control strategies in the dispatching area. The superior dispatching agency is responsible for determining the control objectives and exchanging interactive control information among different areas. Based on the dynamic process of frequency response, three stages should be considered for the AFC method with MSS-MPC:

4) Rapid Frequency Decline

Before the frequency deviation reaches the nadir, the purpose of both the disturbed and undisturbed areas is to suppress the frequency drop in each area. Then, the control objective is to reverse large frequency differences, which should be within the deviation limit allowed by the system.

5) Rapid Frequency Rebound

Before the frequency deviation rebounds to the extreme value, the purpose of disturbed area control is to restore its own frequency, where the control objective is zero frequency deviation. The purpose of the undisturbed area is to recover the system's frequency and tie-line power, where the control objective is zero system frequency deviation and tie-line power increment.

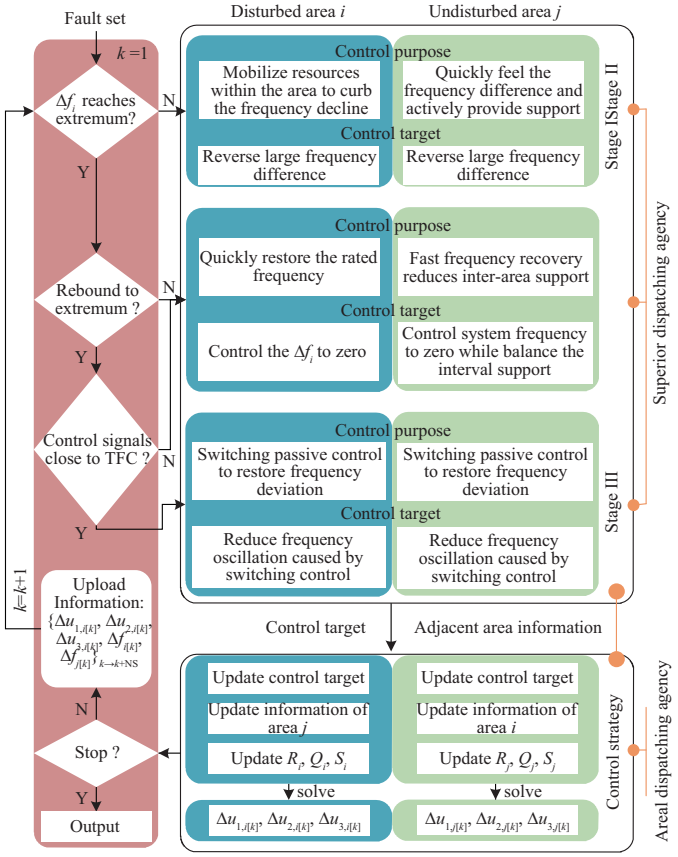

Fig. 2. Three-stage AFC method with MSS-MPC.

6) Slow Frequency Recovery

After the frequency deviation rebounds to the extreme value, active control is switched to passive control at an appropriate time. The purpose of both the disturbed and undisturbed areas is to ensure the stability of the system during the switching process, and the control objective is to reduce the frequency of disturbance arising from switching.

The details of the calculation for all phases in area i are presented below, and those in area j can be obtained by analogy.

In order to achieve three-stage control, the control information exchange between the superior dispatching agency and the areal dispatching agency is important: updating the control objectives set by the superior dispatching agency and the control information transmitted by the adjacent areal dispatching agency, as well as the latest control quantity generated by the areal dispatching agency and the frequency dynamic trend. So, let:

$$\boldsymbol{x}_{i[k+1]}(\Delta f_{j[k+1]}) = \Delta f_{j[k+1]} \tag{20a}$$

Due to different step sizes, the frequency variation of a single step under the same slope may be different. To estimate impacts of frequency dynamics in other areas on the control strategy in this area, the average rate of frequency $\Delta f_{a,j[k+1]}$ is adopted to describe the trend of frequency variation, which works by multiplying elements $(15, 17)$ in $\boldsymbol{A}_{aF,i,1}$ and then superimposing it on $\Delta f_{j[k+1]}$. In the precise prediction interval, let $\boldsymbol{A}_{aF,i,1}(15, 17) = 1$, and then $\Delta f_{a,j[k+1]}$ is as follows:

$$\boldsymbol{x}_{i[k+1]}(\Delta f_{a,j[k+1]}) = \frac{\Delta f_{j[k+NS]} - \Delta f_{j[k]}}{N_1 + \frac{T_{d2,i}}{T_{d1,i}} N_2} \tag{20b}$$

Since the step size of the additional prediction interval is $T_{d2,i}/T_{d1,i}$ times that of the precise prediction interval, then in the additional prediction interval, $\boldsymbol{A}_{aF,i,1}(15,17) = T_{d2,i}/T_{d1,i}$.

During stage II, in order to achieve the control objective, the control target and the target transition matrix are set as follows:

$$\Delta f_{d,i[k+1]} = \Delta f_{d,j[k+1]} = -\frac{H_1}{H_2}\Delta f_{i[k]} \tag{20c}$$

$$\boldsymbol{A}_{\mathrm{D},1} = \boldsymbol{I},\ \boldsymbol{A}_{\mathrm{D},2} = \begin{bmatrix} \boldsymbol{I}^{(n-1)\times(n-1)} & -H_2/H_1 \\ 0 & 1 \end{bmatrix} \tag{20d}$$

where Δf_d is the control target of frequency deviation; the target of area j is derived based on the inertia center frequency.

During stage III, to ensure smooth switching between AFC and TFC, the smooth switching strategy is set as follows:

$$u_{i[k|k]} = \begin{cases} \Delta f_{i[k]} & \Delta t \geq T_{s\mathrm{III}} S_{\mathrm{III}} \\ \Delta f_{i[k]} + \dfrac{T_{s\mathrm{III}} S_{\mathrm{III}}}{T_{sh}} \Delta f_{\mathrm{III}} & \Delta t < T_{s\mathrm{III}} S_{\mathrm{III}} \end{cases} \tag{20e}$$

where $T_{s\mathrm{III}}$ is the simulation step size in stage III; S_{III} is accumulated simulation step in stage III; T_{sh} is the switching delay constant; and Δf_{III} can be calculated by $u_{i[k|k]} - \Delta f_{i[k]}$ at the moment of entering stage III.

V. Case Study and Analysis

The superior performance of the proposed AFC method with MSS-MPC is demonstrated in this section. Two cases are established with a two-area interconnected power system in MATLAB/Simulink:

1) In Case A, the AFC method with MSS-MPC proposed in this paper, the AFC-MPC method, and the TFC method are compared to verify the validity of the proposed method.

2) In Case B, the impacts of various parameters in the proposed method are discussed, and then the direction of further improvement of the method is discussed.

The frequency control model of a two-area interconnected power system is shown in Fig. 3, and most of the parameters of the model are derived from [16]. The main model parameters are given in Appendix D, where the capacity of area A is 3 times that of area B. The capacity proportions of thermal power, hydropower, gas power, and virtual control units in the two areas are all 4:4:1:1. Besides, the parameters of area B are given on the basis of the capacity of area A.

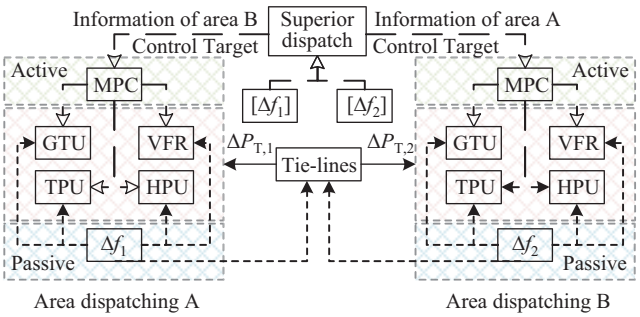

Fig. 3. Frequency control model of two-area interconnected system.

The frequency threshold of low-frequency load shedding is set to 0.5 Hz. In area 1, the valve limit for TPU is ±0.08 p.u., the incremental mechanical power limit for TPU and HPU is ±0.1 p.u., and the incremental power limit for GTUs and VFR resources is 0.01 p.u. Based on the capacity ratio of the two areas, the parameter limitation of area B can be obtained.

A. Validation of the Effectiveness of AFC with MSS-MPC

To verify the effectiveness of the AFC method with MSS-MPC, the AFC method with MPC and the TFC method are compared. It is assumed that a power deficit disturbance occurs in area A at time 0 s. The instantaneous interference power is distributed between the two interconnected areas. Specifically, the interference power distribution is set to 0.1 p.u. in area A, and 0.4 p.u. in area B.

For TFC, the simulation step size is 0.01 s. For AFC with MPC, the sampling step size is 0.01 s, N1 is 120, the control objective of both areas in stage I is 0.01 p.u., the control objective of area A in stage II is zero frequency deviation, the control objective of area B in stage II is zero power deviation on tie-lines, and the switching strategy in stage III is the time when the frequency rebounds to the extremum or zero.

For AFC with MSS-MPC, the shorter sampling step size is 0.01 s, N1 is 10, the longer sampling step size is 0.1 s, N2 is 11, the control objective of both areas in stage I is 0.01 p.u., and the control objective of area B in stage II is zero frequency deviation and zero tie-line power deviation; in stage III, T_{sh} is 10 s and the switching strategy time is 8.5 s. In summary, the control parameters of AFC with MSS-MPC are set as follows:

$$\text{Stage I: } \begin{cases} \boldsymbol{R}_{i,\tau} = \mathrm{diag}(1,1,1) \\ \boldsymbol{S}_{i,\tau} = (1,0,\cdots,0) \\ \boldsymbol{Q}_{i,\tau} = \mathrm{diag}(1,0,\cdots,0) \end{cases} \quad \tau = 1,2,\ i = 1,2.$$

$$\text{Stage II: } \begin{cases} \boldsymbol{R}_{i,\tau} = \mathrm{diag}(1,1,1) \\ \boldsymbol{S}_{i,\tau} = (1,0,\cdots 0.1,0,0,0,0,0) \\ \boldsymbol{Q}_{i,\tau} = \mathrm{diag}(1,0,\cdots,0) \end{cases}$$

$\tau = 1,2,\ i = 1,2.$

The system frequency deviation, the total incremental powers of different areas, the support powers of tie-lines, the incremental power of each FRR, the incremental power of the secondary FRR, and the control signals in different areas with different frequency control methods are shown in Figs. 4–7.

It can be concluded from Fig. 4 that the AFC method with MSS-MPC demonstrates superior performance in mitigating frequency drops and rapidly recovering frequency deviations in the disturbed area, which can provide improved frequency support. Specifically, in stage I, comparable performance is observed in AFC with MSS-MPC or AFC with MPC. However, the maximum frequency deviation is reduced by approximately 0.12 Hz compared to that with TFC, indicating an improvement of 31.57%. In stage II, the AFC method with MSS-MPC addresses both the frequency deviation and the power recovery on the tie-lines in the undisturbed area. Then, compared to TFC and AFC with MPC only considering the tie-line power constraint, the maximum frequency deviation decreases by 0.12 Hz, indicating an improvement of 52%. In

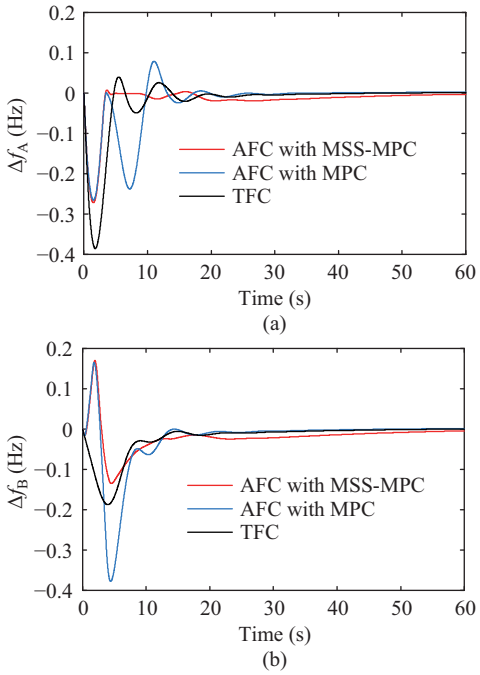

Fig. 4. Frequency deviation curves. (a) Area A. (b) Area B.

stage III, a smooth active-passive control switching strategy is employed in the AFC method with MSS-MPC, resulting in a frequency disturbance of less than 0.02 Hz compared to AFC with MPC, avoiding the risk of additional frequency disturbances and indicating an improvement of 10 times. It should be noted that the frequency deviation is over 0 for 2.41 s with the maximum frequency deviation of 0.16 Hz in the undisturbed area B, which is lower than the maximum positive frequency deviation value set in this study.

It can be concluded from Fig. 5 that the AFC method with MSS-MPC enhances the rates of power increase of both the disturbed and undisturbed areas, thereby strengthening the ability of the undisturbed area to support the disturbed area with power. Specifically, a rapid and significant increase in power may result in frequency overshoot or tie-line power overload. To keep the frequency and the tie-line power within the allowed range, the AFC method significantly changes the direction of the power during regulation, resulting in noticeable additional frequency disturbances after the first swing. Compared to the TFC method, the AFC method with MSS-MPC demonstrates a stronger capability in suppressing these additional frequency disturbances. Then, the power increment in the undisturbed area can be maintained at a higher level for a longer period, indicating stronger power support from the tie-line power. However, the AFC method with MSS-MPC increases the power output of primary frequency regulation, and the power increment of secondary frequency regulation is relatively low and even negative but gradually recovers after switching to passive control. Therefore, future research will focus on AFC further, with both primary and secondary frequency regulation coordinated.

It can be concluded from Figs. 6 and 7 that the AFC with method MSS-MPC is more effective in allocating frequency control resources to different areas. Specifically, in order to

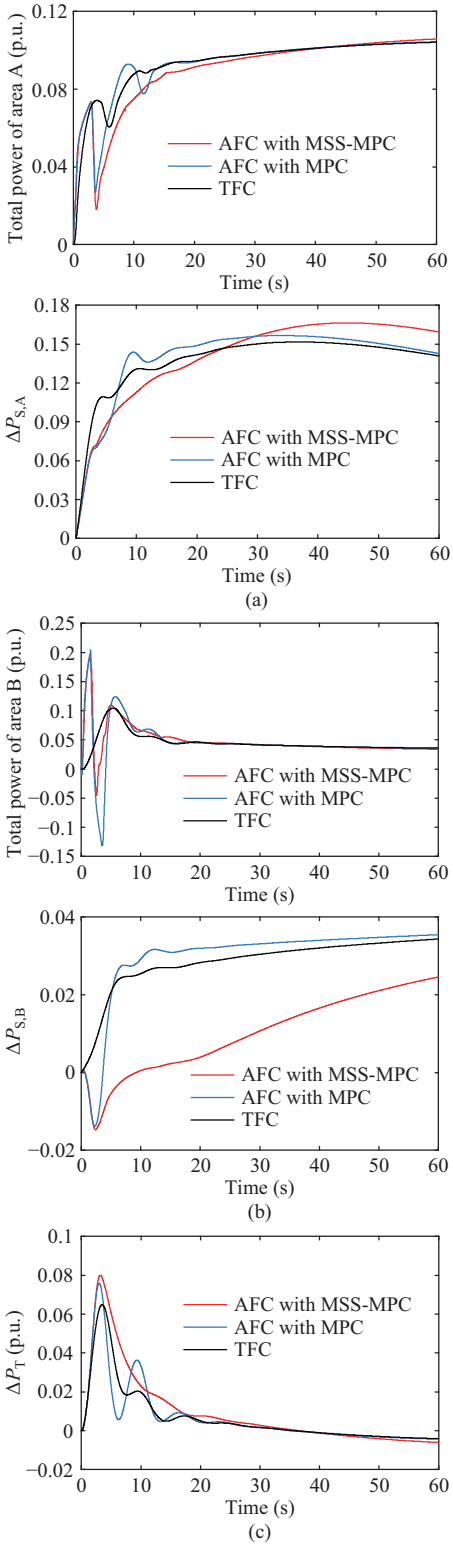

Fig. 5. Total power increment and tie-line power increment. (a) Area A. (b) Area B. (c) Tie-line power from Area B to Area A.

quickly suppress the frequency drop during the early period of the disturbance while minimizing the controller cost, the AFC method with MSS-MPC prioritizes maximizing frequency control resources with faster response compared to TFC. The AFC method with MSS-MPC is more efficient in utilizing flexible resources such as GTUs and VFR resources and reduces the

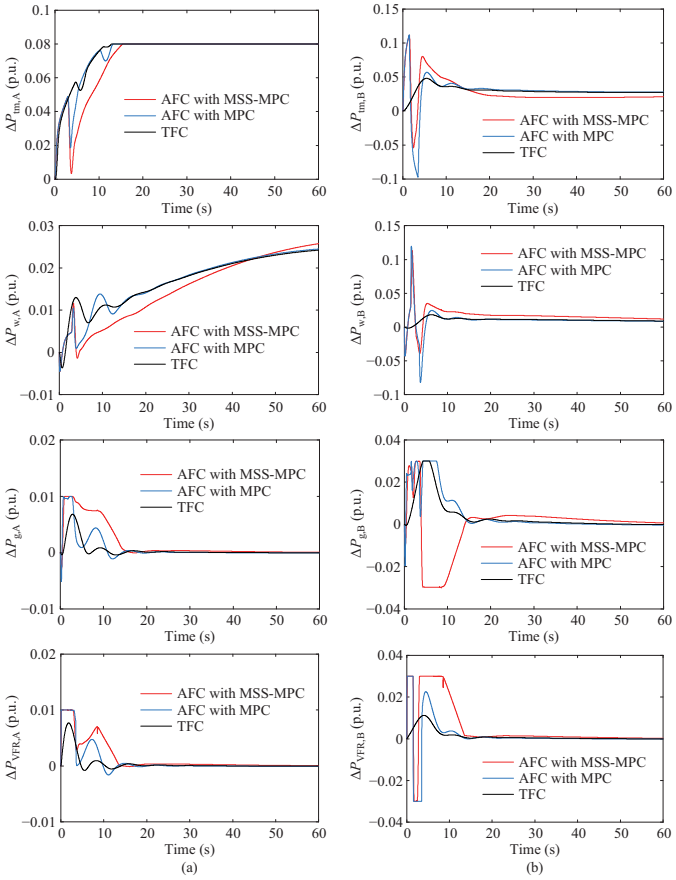

Fig. 6. Incremental power variation of different FRRs. (a) Area A. (b) Area B.

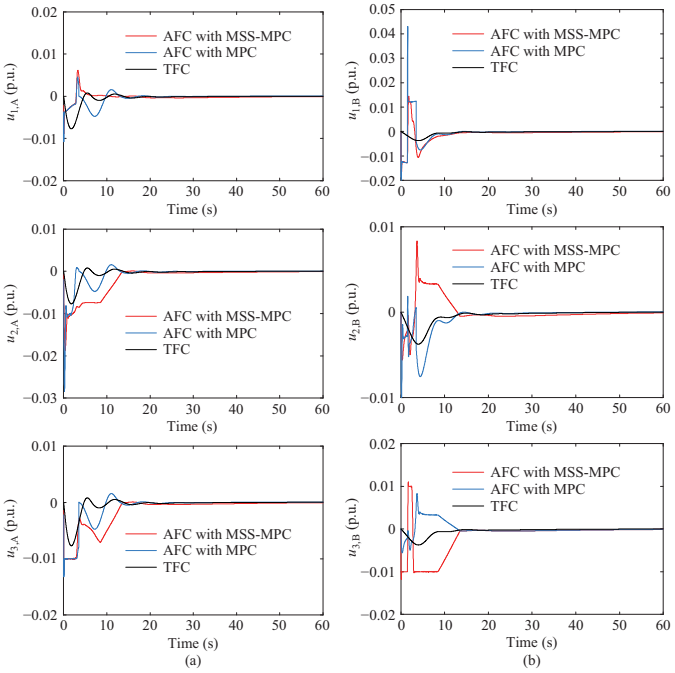

Fig. 7. Control signal variation. (a) Area A. (b) Area B.

inverse-regulation of GTUs and HPUs in the disturbed area. In the middle and late stages of the disturbance, the output of the conventional units gradually increases, progressively displacing the power output from GTUs and VFR resources. The AFC method with MSS-MPC better accommodates the active power regulation time requirements of flexible resources.

B. Discussion and Analysis of Key Parameters

As analyzed in the previous section, the AFC method with MSS-MPC proposed in this paper demonstrates superior performance in active control. This improvement is attributed to the enhanced MSS-MPC algorithm and the optimized switching strategy. In addition, the AFC method with MSS-MPC significantly improves the solution efficiency compared to the TFC method. This section will discuss and analyze the key parameters, such as step size and switching delay, to clarify the advantages and limitations of this study and thus provide directions for future research.

1) Impact Analysis of Forecast Interval Step Size Setting

Low computational efficiency is a key challenge limiting the application of MPC algorithms, with step size being a critical factor influencing computational complexity. In MPC strategy formulation, a smaller step size can improve decision accuracy but also increase model complexity. In turn, computational efficiency can be enhanced by using larger step sizes, but the maximum step size is constrained by the real frequency response model.

Frequency variation curves of different step sizes are shown in Fig. 8 by simulating the frequency response model based on the parameters in Case A. As the simulation step size increases, the simulation accuracy gradually decreases, and the number of steps that can maintain high accuracy decreases accordingly. The additional prediction interval is required to reflect the approximate trend of frequency variation but to improve reliability, and it is still advised to reduce the number of additional prediction steps when larger step sizes are selected. In Case A, when the maximum step size is set to 0.2 s, the prediction horizon can exceed 10 steps. However, when the maximum step size is set to 0.3 s, it is preferable to limit the prediction interval to less than 7 steps. The step sizes and prediction intervals used in this study are determined through simulation experiments, but further research is needed to enable the adaptive selection of these parameters.

To validate the computational efficiency of the proposed algorithm, different prediction intervals are set to compare the solving efficiency of the AFC method with MPC and the AFC method with MSS-MPC, as shown in Table I. The results show that the computation times of both methods increase with the prediction interval. However, for the same prediction interval, ranging from 0.8 s to 1.6 s, the computational time of the improved AFC method with MSS-MPC is 27, 36, and 56 times shorter than that of conventional AFC methods with MSS-MPC, respectively. This demonstrates that the longer the prediction interval, the more obvious the advantage of the AFC method with MSS-MPC will be.

2) Impact Analysis of Switching Moments and Delay Constants

Due to the more aggressive advanced control adopted by the AFC method, a large amount of power will be increased in the early stage of control to suppress the frequency drop. Subse-

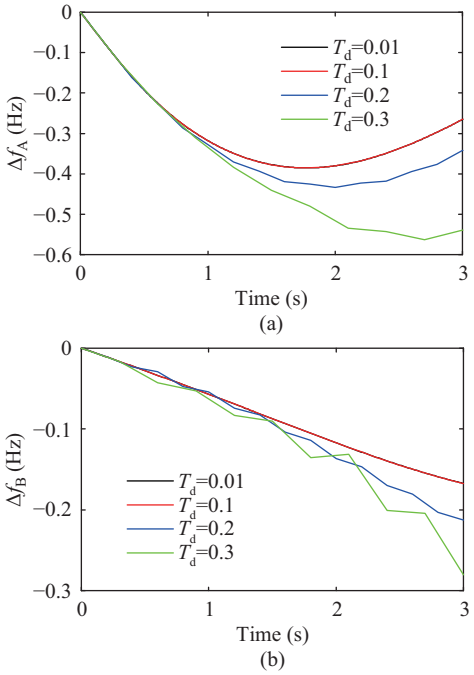

Fig. 8. Frequency variation at different simulation steps. (a) Area A. (b) Area B.

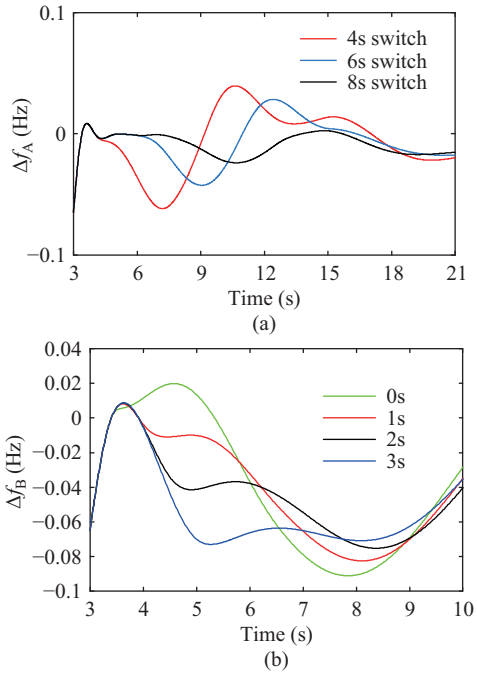

Fig. 9. Frequency variation with different switching moments and delay constants. (a) The impact of switching time. (b) The impact of switching delay.

TABLE I
PERFORMANCE OF THE SYSTEM AT EACH PREDICTION INTERVAL

		Length of prediction interval		
		≥0.8 s	≥1.2 s	≥1.6 s
Conventional AFC	Prediction step	80	120	160
	Computation time	274 s	617 s	1651s
Purposed AFC	Prediction step	16(8+8)	21(10+11)	30(15+15)
	Computation time	<10 s	<17 s	<29 s

quently, in order to prevent frequency overshoot, fast response resources will be controlled to reduce the additional power. Based on this understanding, when the frequency rebounds from the minimum to zero, it may still be rapidly changing. If passive control is suddenly applied at this moment, it may create a new power imbalance, leading to anomalous frequency fluctuations.

To verify the effect of the active-to-passive switching moments and delay constants on frequency variability, simulations are performed using the same switching moments but different delay constants. As shown in Fig. 9, it indicates that the later switching occurs, the additional frequency disturbance induced by switching will be smaller. Moreover, for the same switching moment, a longer switching delay results in a smaller additional frequency disturbance. In this study, the switching strategy parameters are selected through simulation, and the proposed switching strategy is demonstrated by the analysis above. However, its effectiveness is related to parameter selection, which is within a certain range only. This topic will not be further explored. More in-depth exploration will be conducted on the selection of switching functions and the optimal solution of switching parameters in the future.

VI. CONCLUSION

In this paper, the wide-area AFC method with MSS-MPC is proposed to address the limitations of existing AFC methods in terms of solution efficiency and control effectiveness. Three-stage control for the AFC method is improved, and the key parameters are discussed. The main conclusion is as follows:

1) The proposed MSS-MPC algorithm based on multi-step-size LQR can utilize both shorter and longer step sizes to ensure solution accuracy and significantly enlarge the prediction interval. It can conduct advanced decision-making on a larger time scale with fewer steps only. Compared with conventional AFC methods, it is easier to overcome the resource inversion characteristic and improve solution efficiency by tens of times.

2) The proposed three-stage AFC method with MSS-MPC achieves an iterative solution and target information exchange based on two-level scheduling and reduces additional frequency disturbances by using active-passive smooth switching functions. Compared with conventional AFC methods, the power allocation of FRRs is more reasonable, and the frequency suppression and recovery control effects are better.

3) The algorithm parameters of the AFC method with MSS-MPC can be obtained through simulation. Within a certain range, the larger the additional prediction step size is, or the smaller the number of steps at the same prediction interval, the lower computational complexity will be; the larger the active-passive smooth switching time and delay constant, the smaller the frequency disturbance arising from switching will be.

In summary, this paper verifies the feasibility of the AFC method with MSS-MPC. Further research will be conducted on MPC algorithms with more step sizes or adaptive variable step sizes, as well as AFC techniques based on other forms of improved MPC.

APPENDIX

A. Appendix A

The expressions of state matrix $\boldsymbol{A}_i$ and control matrix $\boldsymbol{B}_i$ are as follows:

$$\boldsymbol{A}=\begin{bmatrix}\boldsymbol{A}_{11} & \boldsymbol{A}_{12} & \boldsymbol{A}_{13} & \boldsymbol{A}_{14}\\ 0 & \boldsymbol{A}_{22} & 0 & \boldsymbol{A}_{24}\\ 0 & 0 & \boldsymbol{A}_{33} & 0\\ \boldsymbol{A}_{41} & \boldsymbol{A}_{42} & \boldsymbol{A}_{43} & \boldsymbol{A}_{44}\end{bmatrix},\ \boldsymbol{B}_{11}=\begin{bmatrix}\boldsymbol{B}_{11}\\ \boldsymbol{B}_{21}\\ \boldsymbol{B}_{31}\\ 0\end{bmatrix} \tag{A1}$$

$$\boldsymbol{A}_{11}=\begin{bmatrix}-\frac{D_i}{2H_i} & \frac{1}{2H_i} & 0 & 0\\ 0 & -\frac{1}{T_{\mathrm{tr,i}}} & \frac{T_{\mathrm{th,i}}-K_{\mathrm{tr,i}}T_{\mathrm{tr,i}}}{T_{\mathrm{tr,i}}T_{\mathrm{th,i}}} & \frac{K_{\mathrm{tr,i}}}{T_{\mathrm{th,i}}}\\ 0 & 0 & -\frac{1}{T_{\mathrm{th,i}}} & \frac{1}{T_{\mathrm{th,i}}}\\ 0 & 0 & 0 & -\frac{1}{T_{\mathrm{g},i}}\end{bmatrix}$$

$$\boldsymbol{A}_{12}=\begin{bmatrix}\frac{1}{2H_i} & 0 & 0\\ 0 & 0 & 0\\ 0 & 0 & 0\\ 0 & 0 & 0\end{bmatrix} \tag{A2}$$

$$\boldsymbol{A}_{13}=\begin{bmatrix}\frac{1}{2H_i} & 0 & 0 & 0 & \frac{1}{2H_i}\\ 0 & 0 & 0 & 0 & 0\\ 0 & 0 & 0 & 0 & 0\\ 0 & 0 & 0 & 0 & 0\end{bmatrix}$$

$$\boldsymbol{A}_{14}=\begin{bmatrix}-\frac{1}{2H_i} & 0 & 0 & -\frac{1}{2H_i} & 0\\ 0 & 0 & 0 & 0 & 0\\ 0 & 0 & 0 & 0 & 0\\ 0 & \frac{k_{1,i}}{T_{\mathrm{g},i}} & 0 & 0 & 0\end{bmatrix} \tag{A3}$$

$$\boldsymbol{A}_{22}=\begin{bmatrix}-\frac{1}{0.5T_{\mathrm{w,i}}} & \frac{(R_{\mathrm{wt,i}}/R_{\mathrm{wp},i})T_{\mathrm{wr,i}}+T_{\mathrm{w},i}}{0.5(R_{\mathrm{wt,i}}/R_{\mathrm{wp},i})T_{\mathrm{wr,i}}T_{\mathrm{w},i}} & -\frac{T_{\mathrm{wg},i}-T_{\mathrm{wr,i}}}{0.5(R_{\mathrm{wt,i}}/R_{\mathrm{wp},i})T_{\mathrm{wr,i}}T_{\mathrm{wg},i}}\\ 0 & -\frac{1}{(R_{\mathrm{wt,i}}/R_{\mathrm{wp},i})T_{\mathrm{wr,i}}} & \frac{T_{\mathrm{wg},i}-T_{\mathrm{wr,i}}}{(R_{\mathrm{wt,i}}/R_{\mathrm{wp},i})T_{\mathrm{wr,i}}T_{\mathrm{wg},i}}\\ 0 & 0 & -\frac{1}{T_{\mathrm{wg},i}}\end{bmatrix} \tag{A4}$$

$$\boldsymbol{A}_{24}=\begin{bmatrix}0 & -\frac{k_{2,i}}{0.5T_{\mathrm{wg},i}(R_{\mathrm{wt,i}}/R_{\mathrm{wp},i})} & 0 & 0 & 0\\ 0 & \frac{k_{2,i}}{T_{\mathrm{wg},i}(R_{\mathrm{wt,i}}/R_{\mathrm{wp},i})} & 0 & 0 & 0\\ 0 & \frac{k_{2,i}}{T_{\mathrm{wg},i}} & 0 & 0 & 0\end{bmatrix} \tag{A5}$$

$$\boldsymbol{A}_{33}=\begin{bmatrix}-\frac{1}{T_{\mathrm{CD},i}} & \frac{1}{T_{\mathrm{CD},i}} & 0 & 0 & 0\\ 0 & -\frac{1}{T_{\mathrm{F},i}} & \frac{Y_i-T_{\mathrm{CR},i}}{Y_iT_{\mathrm{F},i}} & \frac{T_{\mathrm{CR},i}}{T_{\mathrm{F},i}}\frac{b_i-c_iX_i}{b_iY_i} & 0\\ 0 & 0 & -\frac{1}{Y_i} & \frac{b_i-c_iX_i}{b_iY_i} & 0\\ 0 & 0 & 0 & -\frac{c_i}{b_i} & 0\\ 0 & 0 & 0 & 0 & -\frac{1}{T_{\mathrm{VFR},i}}\end{bmatrix} \tag{A6}$$

$$\boldsymbol{A}_{41}=\begin{bmatrix}2\pi\sum_{j=1,j\neq i}^{N}T_{ij} & 0 & 0 & 0\\ k_{\mathrm{tI}}B_i-\frac{k_{\mathrm{tP}}B_iD_i}{2H_i}+k_{\mathrm{tP}}\alpha_i2\pi\sum_{j=1,j\neq i}^{N}T_{ij} & \frac{k_{\mathrm{tP}}B_i}{2H_i} & 0 & 0\\ 0 & 0 & 0 & 0\\ 0 & 0 & 0 & 0\\ 0 & 0 & 0 & 0\end{bmatrix} \tag{A7}$$

$$\boldsymbol{A}_{42}=\begin{bmatrix}0 & 0 & 0\\ \frac{k_{\mathrm{tP}}B_i}{2H_i} & 0 & 0\\ 0 & 0 & 0\\ 0 & 0 & 0\\ 0 & 0 & 0\end{bmatrix},\ \boldsymbol{A}_{43}=\begin{bmatrix}0 & 0 & 0 & 0 & 0\\ \frac{k_{\mathrm{tP}}B_i}{2H_i} & 0 & 0 & 0 & \frac{k_{\mathrm{tP}}B_i}{2H_i}\\ 0 & 0 & 0 & 0 & 0\\ 0 & 0 & 0 & 0 & 0\\ 0 & 0 & 0 & 0 & 0\end{bmatrix} \tag{A8}$$

$$\boldsymbol{A}_{44}=\begin{bmatrix}0 & 0 & -2\pi\sum_{j=1,j\neq i}^{N}T_{ij} & 0 & 0\\ k_{\mathrm{tI}}\alpha_i-\frac{k_{\mathrm{tP}}B_i}{2H_i} & 0 & -k_{\mathrm{tP}}\alpha_i2\pi\sum_{j=1,j\neq i}^{N}T_{ij} & -\frac{k_{\mathrm{tP}}B_i}{2H_i} & 0\\ 0 & 0 & 0 & 0 & 0\\ 0 & 0 & 0 & 0 & 0\\ 0 & 0 & 0 & 0 & 0\end{bmatrix} \tag{A9}$$

$$\boldsymbol{B}_{11}=\begin{bmatrix}0 & 0 & 0 & 0\\ 0 & 0 & 0 & 0\\ -\frac{1}{R_{\mathrm{g},i}T_{\mathrm{g},i}} & 0 & 0 & 0\\ 0 & 0 & 0 & 0\end{bmatrix}$$

$$\boldsymbol{B}_{21}=\begin{bmatrix}\frac{2}{T_{\mathrm{wg},i}R_{\mathrm{w},i}(R_{\mathrm{wt,i}}/R_{\mathrm{wp},i})} & 0 & 0 & 0\\ \frac{2}{T_{\mathrm{wg},i}R_{\mathrm{w},i}(R_{\mathrm{wt,i}}/R_{\mathrm{wp},i})} & 0 & 0 & 0\\ -\frac{1}{T_{\mathrm{wg},i}R_{\mathrm{w},i}} & 0 & 0 & 0\end{bmatrix} \tag{A10}$$

$$\boldsymbol{B}_{21}=\begin{bmatrix}0 & 0 & 0 & 0\\ 0 & -\frac{T_{\mathrm{CR},i}}{T_{\mathrm{F},i}}\frac{a_iX_i}{R_{\mathrm{e},i}b_iY_i} & 0 & 0\\ 0 & -\frac{a_iX_i}{R_{\mathrm{e},i}b_iY_i} & 0 & 0\\ 0 & -\frac{a_i}{R_{\mathrm{e},i}b_i} & 0 & 0\\ 0 & 0 & -\frac{1}{T_{\mathrm{VFR},i}R_{\mathrm{VFR},i}} & 0\end{bmatrix} \tag{A11}$$

B. Appendix B

The compact form of the state equation for the precise prediction interval and the additional prediction interval is derived using the inductive method, and the process is as follows.

According to (11), within the precise prediction interval, at the $k+1$th moment:

$$\boldsymbol{x}_{\mathrm{a},i[k+1|k]}=\boldsymbol{A}_{\mathrm{aF},i,1}\boldsymbol{x}_{\mathrm{a},i[k|k]}+\boldsymbol{B}_{\mathrm{aG},i,1}\Delta\boldsymbol{u}_{i[k|k]} \tag{B1}$$

the $k+2$th moment:

$$\begin{aligned}\boldsymbol{x}_{\mathrm{a},i[k+2|k]}&=\boldsymbol{A}_{\mathrm{aF},i,1}\boldsymbol{x}_{\mathrm{a}[k+1|k]}+\boldsymbol{B}_{\mathrm{aG},i,1}\Delta\boldsymbol{u}_{i[k+1|k]}\\&=\boldsymbol{A}_{\mathrm{aF},i,1}^2\boldsymbol{x}_{\mathrm{a},i[k|k]}+\boldsymbol{A}_{\mathrm{aF},i,1}\boldsymbol{B}_{\mathrm{aG},i,1}\Delta\boldsymbol{u}_{i[k|k]}\\&\quad+\boldsymbol{B}_{\mathrm{aG},i,1}\Delta\boldsymbol{u}_{i[k+1|k]}\end{aligned} \tag{B2}$$

the $k+3$th moment:

$$\begin{aligned}\boldsymbol{x}_{\mathrm{a},i[k+3|k]}&=\boldsymbol{A}_{\mathrm{aF},i,1}\boldsymbol{x}_{\mathrm{a},i[k+2|k]}+\boldsymbol{B}_{\mathrm{aG},i,1}\Delta\boldsymbol{u}_{i[k+2|k]}\\&=\boldsymbol{A}_{\mathrm{aF},i,1}^3\boldsymbol{x}_{\mathrm{a},i[k|k]}+\boldsymbol{A}_{\mathrm{aF},i,1}^2\boldsymbol{B}_{\mathrm{aG},i,1}\Delta\boldsymbol{u}_{i[k|k]}\\&\quad+\boldsymbol{A}_{\mathrm{aF},i,1}\boldsymbol{B}_{\mathrm{aG},i,1}\Delta\boldsymbol{u}_{i[k+1|k]}\\&\quad+\boldsymbol{B}_{\mathrm{aG},i,1}\Delta\boldsymbol{u}_{i[k+2|k]}\end{aligned} \tag{B3}$$

Therefore, according to mathematical induction, at the $k+N_1$th moment:

$$\begin{aligned}\boldsymbol{x}_{\mathrm{a},i[k+N_1|k]}&=\boldsymbol{A}_{\mathrm{aF},i,1}\boldsymbol{x}_{\mathrm{a},i[k+N_1-1|k]}+\boldsymbol{B}_{\mathrm{aG},i,1}\Delta\boldsymbol{u}_{i[k+N_1-1|k]}\\&=\boldsymbol{A}_{\mathrm{aF},i,1}^{N_1}\boldsymbol{x}_{\mathrm{a},i[k|k]}+\boldsymbol{A}_{\mathrm{aF},i,1}^{N_1-1}\boldsymbol{B}_{\mathrm{aG},i,1}\Delta\boldsymbol{u}_{i[k|k]}\\&\quad+\boldsymbol{A}_{\mathrm{aF},i,1}^{N_1-2}\boldsymbol{B}_{\mathrm{aG},i,1}\Delta\boldsymbol{u}_{i[k+1|k]}+\cdots\\&\quad+\boldsymbol{A}_{\mathrm{aF},i,1}\boldsymbol{B}_{\mathrm{aG},i,1}\Delta\boldsymbol{u}_{i[k+N-2|k]}\\&\quad+\boldsymbol{B}_{\mathrm{aG},i,1}\Delta\boldsymbol{u}_{i[k+N-1|k]}\end{aligned} \tag{B4}$$

Also according to (11), within the additional prediction interval, at the $k+N_1+1$th moment:

$$\boldsymbol{x}_{\mathrm{a},i[k+N_1+1|k]}=\boldsymbol{A}_{\mathrm{aF},i,2}\boldsymbol{x}_{\mathrm{a},i[k+N_1|k]}+\boldsymbol{B}_{\mathrm{aG},i,2}\Delta\boldsymbol{u}_{i[k+N_i|k]} \tag{B5}$$

the $k+N_1+2$th moment:

$$\begin{aligned}&\boldsymbol{x}_{\mathrm{a},i[k+N_1+2|k]}\\&=\boldsymbol{A}_{\mathrm{aF},i,2}\boldsymbol{x}_{\mathrm{a},i[k+N_1+2|k]}+\boldsymbol{B}_{\mathrm{aG},i,2}\Delta\boldsymbol{u}_{i[k+N_1+2|k]}\\&=\boldsymbol{A}_{\mathrm{aF},i,2}^{2}\boldsymbol{x}_{\mathrm{a},i[k+N_1|k]}+\boldsymbol{A}_{\mathrm{aF},i,2}\boldsymbol{B}_{\mathrm{aG},i,2}\Delta\boldsymbol{u}_{i[k+N_1|k]}\\&\quad+\boldsymbol{B}_{\mathrm{aG},i,2}\Delta\boldsymbol{u}_{i[k+N_1+1|k]}\end{aligned}\tag{B6}$$

the $k+N_1+3$th moment:

$$\begin{aligned}&\boldsymbol{x}_{\mathrm{a},i[k+N_1+3|k]}\\&=\boldsymbol{A}_{\mathrm{aF}.i.2}\boldsymbol{x}_{\mathrm{a}[k+N_1+2|k]}+\boldsymbol{B}_{\mathrm{aG},i,2}\Delta\boldsymbol{u}_{[k+N_1+2|k]}\\&=\boldsymbol{A}_{\mathrm{aF},i,2}^{3}\boldsymbol{x}_{\mathrm{a}[k+N_1|k]}+\boldsymbol{A}_{\mathrm{aF},i,2}^{2}\boldsymbol{B}_{\mathrm{aG},i,2}\Delta\boldsymbol{u}_{[k+N_1|k]}\\&\quad+\boldsymbol{A}_{\mathrm{aF},i,2}\boldsymbol{B}_{\mathrm{aG},i,2}\Delta\boldsymbol{u}_{i[k+N_1+1|k]}+\boldsymbol{B}_{\mathrm{aG},i,2}\Delta\boldsymbol{u}_{[k+N_1+2|k]}\end{aligned}\tag{B7}$$

Therefore, according to inductive method, at the $k+N_1+N_2$th moment:

$$\begin{aligned}&\boldsymbol{x}_{\mathrm{a},i[k+NS|k]}\\&=\boldsymbol{A}_{\mathrm{aF},i,2}^{N_2}\boldsymbol{x}_{\mathrm{a},i[k+N_1|k]}+\boldsymbol{A}_{\mathrm{aF},i,2}\boldsymbol{B}_{\mathrm{aG},i,2}\Delta\boldsymbol{u}_{i[k+N_1|k]}\\&\quad+\boldsymbol{B}_{\mathrm{aG},i,2}\Delta\boldsymbol{u}_{i[k+N_1+1|k]}\\&=\boldsymbol{A}_{\mathrm{aF},i,2}^{N_2}\boldsymbol{A}_{\mathrm{aF},i,1}^{N_1}\boldsymbol{x}_{\mathrm{a},i[k|k]}+\boldsymbol{A}_{\mathrm{aF},i,2}^{N_2}\boldsymbol{A}_{\mathrm{aF}1}^{N_1-1}\boldsymbol{B}_{\mathrm{aG}1}\Delta\boldsymbol{u}_{[k|k]}\\&\quad+\boldsymbol{A}_{\mathrm{aF},i,2}^{N_2}\boldsymbol{A}_{\mathrm{aF},i,1}^{N_1-2}\boldsymbol{B}_{\mathrm{aG},i,1}\Delta\boldsymbol{u}_{i[k+1|k]}+\cdots\\&\quad+\boldsymbol{A}_{\mathrm{aF},i,2}^{N_2}\boldsymbol{A}_{\mathrm{aF},i,1}\boldsymbol{B}_{\mathrm{aG},i,1}\Delta\boldsymbol{u}_{i[k+N_1-2|k]}\\&\quad+\boldsymbol{A}_{\mathrm{aF},i,2}^{N_2}\boldsymbol{B}_{\mathrm{aG},i,1}\Delta\boldsymbol{u}_{i[k+N_1-1|k]}\\&\quad+\boldsymbol{A}_{\mathrm{aF},i,2}^{N_2-1}\boldsymbol{B}_{\mathrm{aG},i,2}\Delta\boldsymbol{u}_{i[k+N_1|k]}\\&\quad+\boldsymbol{A}_{\mathrm{aF},i,2}^{N_2-2}\boldsymbol{B}_{\mathrm{aG},i,2}\Delta\boldsymbol{u}_{[k+N_1+1|k]}+\cdots\\&\quad+\boldsymbol{A}_{\mathrm{aF},i,2}\boldsymbol{B}_{\mathrm{aG},i,2}\Delta\boldsymbol{u}_{i[k+NS-2|k]}\\&\quad+\boldsymbol{B}_{\mathrm{aG},i,2}\Delta\boldsymbol{u}_{i[k+NS-1|k]}\end{aligned}\tag{B8}$$

When (B1)–(B8) are combined, the form shown in (14) can be deduced.

The following is to prove the correctness of the inductive results based on mathematical induction. Since the processes of using the inductive method twice in Appendix B are the same, only mathematical induction is used here to prove the correctness of (B1)–(B4), which can be directly applied to the proving of (B5)–(B8). For (B1)–(B4), the following problems exist:

Given

$$\boldsymbol{x}_{\mathrm{a},i[k+1|k]}=\boldsymbol{A}_{\mathrm{aF},i,1}\boldsymbol{x}_{\mathrm{a},i[k|k]}+\boldsymbol{B}_{\mathrm{aG},i,1}\Delta\boldsymbol{u}_{i[k|k]}\tag{B9}$$

$$\boldsymbol{A}_{\mathrm{aF},i,1}^{\mathrm{Q}}=\begin{cases}0 & Q<1\\ \boldsymbol{A}_{\mathrm{aF},i,1}^{\mathrm{Q}} & Q\geq 1\end{cases}$$

$$\Delta\boldsymbol{u}_{i[k+\mathrm{Z}|k]}=\begin{cases}0 & Z<0\\ \Delta\boldsymbol{u}_{i[k+\mathrm{Z}|k]} & Z\geq 0\end{cases}\tag{B10}$$

Prove that

$$\begin{aligned}&\boldsymbol{x}_{\mathrm{a},i[k+N_1|k]}\\&=\boldsymbol{A}_{\mathrm{aF},i,1}\boldsymbol{x}_{\mathrm{a},i[k+N_1-1|k]}+\boldsymbol{B}_{\mathrm{aG},i,1}\Delta\boldsymbol{u}_{i[k+N_1-1|k]}\\&=\boldsymbol{A}_{\mathrm{aF},i,1}^{N_1}\boldsymbol{x}_{\mathrm{a},i[k|k]}+\boldsymbol{A}_{\mathrm{aF},i,1}^{N_1-1}\boldsymbol{B}_{\mathrm{aG},i,1}\Delta\boldsymbol{u}_{i[k|k]}\\&\quad+\boldsymbol{A}_{\mathrm{aF},i,1}^{N_1-2}\boldsymbol{B}_{\mathrm{aG},i,1}\Delta\boldsymbol{u}_{i[k+1|k]}\\&\quad+\cdots+\boldsymbol{A}_{\mathrm{aF},i,1}\boldsymbol{B}_{\mathrm{aG},i,1}\Delta\boldsymbol{u}_{i[k+N_1-2|k]}\\&\quad+\boldsymbol{B}_{\mathrm{aG},i,1}\Delta\boldsymbol{u}_{i[k+N_1-1|k]}\end{aligned}\tag{B11}$$

The proving process is as follows:

1) When $N_1=1$, thus

$$\begin{aligned}\boldsymbol{x}_{\mathrm{a},i[k+1|k]}&=\boldsymbol{A}_{\mathrm{aF},i,1}^{1}\boldsymbol{x}_{\mathrm{a},i[k|k]}+\boldsymbol{A}_{\mathrm{aF},i,1}^{0}\boldsymbol{B}_{\mathrm{aG},i,1}\Delta\boldsymbol{u}_{i[k|k]}\\&\quad+\boldsymbol{A}_{\mathrm{aF},i,1}^{-1}\boldsymbol{B}_{\mathrm{aG},i,1}\Delta\boldsymbol{u}_{i[k+1|k]}\\&\quad+\cdots+\boldsymbol{A}_{\mathrm{aF},i,1}\boldsymbol{B}_{\mathrm{aG},i,1}\Delta\boldsymbol{u}_{i[k+-2|k]}\\&\quad+\boldsymbol{B}_{\mathrm{aG},i,1}\Delta\boldsymbol{u}_{i[k+N_1-1|k]}\\&=\boldsymbol{A}_{\mathrm{aF},i,1}\boldsymbol{x}_{\mathrm{a},i[k|k]}+\boldsymbol{B}_{\mathrm{aG},i,1}\Delta\boldsymbol{u}_{i[k|k]}\end{aligned}\tag{B12}$$

2) The Proving Process Is as Follows: Assume That When $N_1=r$ ($r\geq 1$ and $r\in N^{+}$), the following equation holds:

$$\begin{aligned}\boldsymbol{x}_{\mathrm{a},i[k+r|k]}&=\boldsymbol{A}_{\mathrm{aF},i,1}\boldsymbol{x}_{\mathrm{a},i[k+r-1|k]}+\boldsymbol{B}_{\mathrm{aG},i,1}\Delta\boldsymbol{u}_{i[k+r-1|k]}\\&=\boldsymbol{A}_{\mathrm{aF},i,1}^{r}\boldsymbol{x}_{\mathrm{a},i[k|k]}+\boldsymbol{A}_{\mathrm{aF},i,1}^{r-1}\boldsymbol{B}_{\mathrm{aG},i,1}\Delta\boldsymbol{u}_{i[k|k]}\\&\quad+\boldsymbol{A}_{\mathrm{aF},i,1}^{r-2}\boldsymbol{B}_{\mathrm{aG},i,1}\Delta\boldsymbol{u}_{i[k+1|k]}\\&\quad+\cdots+\boldsymbol{A}_{\mathrm{aF},i,1}\boldsymbol{B}_{\mathrm{aG},i,1}\Delta\boldsymbol{u}_{i[k+r-2|k]}\\&\quad+\boldsymbol{B}_{\mathrm{aG},i,1}\Delta\boldsymbol{u}_{i[k+r-1|k]}\end{aligned}\tag{B13}$$

3) And When $N_1=r+1$,

$$\boldsymbol{x}_{\mathrm{a},i[k+r+1|k]}=\boldsymbol{A}_{\mathrm{aF},i,1}\boldsymbol{x}_{\mathrm{a},i[k+r|k]}+\boldsymbol{B}_{\mathrm{aG},i,1}\Delta\boldsymbol{u}_{i[k+r|k]}\tag{B14}$$

By substituting (B13) into (B14), and we obtain

$$\begin{aligned}\boldsymbol{x}_{\mathrm{a},i[k+r+1|k]}&=\boldsymbol{A}_{\mathrm{aF},i,1}\boldsymbol{x}_{\mathrm{a},i[k+r|k]}+\boldsymbol{B}_{\mathrm{aG},i,1}\Delta\boldsymbol{u}_{i[k+r|k]}\\&=\boldsymbol{A}_{\mathrm{aF},i,1}\begin{pmatrix}\boldsymbol{A}_{\mathrm{aF},i,1}^{r}\boldsymbol{x}_{\mathrm{a},i[k|k]}\\+\boldsymbol{A}_{\mathrm{aF},i,1}^{r-1}\boldsymbol{B}_{\mathrm{aG},i,1}\Delta\boldsymbol{u}_{i[k|k]}\\+\boldsymbol{A}_{\mathrm{aF},i,1}^{r-2}\boldsymbol{B}_{\mathrm{aG},i,1}\Delta\boldsymbol{u}_{i[k+1|k]}\\+\cdots\\+\boldsymbol{A}_{\mathrm{aF},i,1}\boldsymbol{B}_{\mathrm{aG},i,1}\Delta\boldsymbol{u}_{i[k+r-2|k]}\\+\boldsymbol{B}_{\mathrm{aG},i,1}\Delta\boldsymbol{u}_{i[k+r-1|k]}\end{pmatrix}\\&\quad+\boldsymbol{B}_{\mathrm{aG},i,1}\Delta\boldsymbol{u}_{i[k+r|k]}\\&=\boldsymbol{A}_{\mathrm{aF},i,1}^{r+1}\boldsymbol{x}_{\mathrm{a},i[k|k]}+\boldsymbol{A}_{\mathrm{aF},i,1}^{r}\boldsymbol{B}_{\mathrm{aG},i,1}\Delta\boldsymbol{u}_{i[k|k]}\\&\quad+\boldsymbol{A}_{\mathrm{aF},i,1}^{r-1}\boldsymbol{B}_{\mathrm{aG},i,1}\Delta\boldsymbol{u}_{i[k+1|k]}\\&\quad+\cdots+\boldsymbol{A}_{\mathrm{aF},i,1}\boldsymbol{B}_{\mathrm{aG},i,1}\Delta\boldsymbol{u}_{i[k+r-1|k]}\\&\quad+\boldsymbol{B}_{\mathrm{aG},i,1}\Delta\boldsymbol{u}_{i[k+r|k]}\end{aligned}\tag{B15}$$

In conclusion, by mathematical induction, it can be known that for any $N_1\in\boldsymbol{N}^{+}$, the following formula holds:

$$\begin{aligned}\boldsymbol{x}_{\mathrm{a},i[k+N_1|k]}&=\boldsymbol{A}_{\mathrm{aF},i,1}\boldsymbol{x}_{\mathrm{a},i[k+N_1-1|k]}+\boldsymbol{B}_{\mathrm{aG},i,1}\Delta\boldsymbol{u}_{i[k+N_1-1|k]}\\&=\boldsymbol{A}_{\mathrm{aF},i,1}^{N_1}\boldsymbol{x}_{\mathrm{a},i[k|k]}+\boldsymbol{A}_{\mathrm{aF},i,1}^{N_1-1}\boldsymbol{B}_{\mathrm{aG},i,1}\Delta\boldsymbol{u}_{i[k|k]}\\&\quad+\boldsymbol{A}_{\mathrm{aF},i,1}^{N_1-2}\boldsymbol{B}_{\mathrm{aG},i,1}\Delta\boldsymbol{u}_{i[k+1|k]}+\cdots\\&\quad+\boldsymbol{A}_{\mathrm{aF},i,1}\boldsymbol{B}_{\mathrm{aG},i,1}\Delta\boldsymbol{u}_{i[k+N_1-2|k]}\\&\quad+\boldsymbol{B}_{\mathrm{aG},i,1}\Delta\boldsymbol{u}_{i[k+N_1-1|k]}\end{aligned}\tag{B16}$$

Proving is completed.

C. Appendix C

The compact form of constraint (17) is derived based on the inductive method, as follows:

According to (17), within the precise prediction interval, the constraint condition can be written as:

$$\begin{cases}\boldsymbol{M}_{i[k]}\boldsymbol{x}_{\mathrm{a},i[k|k]}+\boldsymbol{W}_{i[k]}\Delta\boldsymbol{u}_{i[k|k]}\leq\boldsymbol{\beta}_{i[k]}\\ \boldsymbol{M}_{i[k+1]}\boldsymbol{x}_{\mathrm{a},i[k+1|k]}+\boldsymbol{W}_{i[k+1]}\Delta\boldsymbol{u}_{i[k+1|k]}\leq\boldsymbol{\beta}_{i[k+1]}\\ \cdots\\ \boldsymbol{M}_{i[k+N]}\boldsymbol{x}_{\mathrm{a},i[k+N_1|k]}+\boldsymbol{W}_{[k+N_1]}\Delta\boldsymbol{u}_{[k+N_1|k]}\leq\boldsymbol{\beta}_{[k+N_1]}\end{cases}\tag{C1}$$

Meanwhile, in the additional prediction interval, the constraints can be written as:

$$\begin{cases} \boldsymbol{M}_{i[k+N+1]}\boldsymbol{x}_{\mathrm{a},i[k+N+1|k]} + \boldsymbol{W}_{i[k+N+1]}\Delta\boldsymbol{u}_{i[k+N+1|k]} \\ \quad \leq \boldsymbol{\beta}_{i[k+N+1]} \\ \boldsymbol{M}_{i[k+N+2]}\boldsymbol{x}_{\mathrm{a},i[k+N+2|k]} + \boldsymbol{W}_{i[k+N+2]}\Delta\boldsymbol{u}_{i[k+N+2|k]} \\ \quad \leq \boldsymbol{\beta}_{i[k+N+2]} \\ \cdots \\ \boldsymbol{M}_{i[k+NS-1]}\boldsymbol{x}_{\mathrm{a},i[k+NS-1|k]} + \boldsymbol{W}_{i[k+NS-1]}\Delta\boldsymbol{u}_{i[k+NS-1|k]} \\ \quad \leq \boldsymbol{\beta}_{i[k+NS-1]} \end{cases} \tag{C2}$$

At the end of the additional prediction interval, the constraints can be written as:

$$\boldsymbol{M}_{i[k+NS]}\boldsymbol{x}_{\mathrm{a},i[k+NS|k]} \leq \boldsymbol{\beta}_{i[k+NS]} \tag{C3}$$

Combining (C1)-(C3):

$$\begin{aligned} &\begin{bmatrix} \boldsymbol{M}_{i[k]} \\ 0 \\ 0 \\ \cdots \\ 0 \end{bmatrix} \boldsymbol{x}_{a,i[k|k]} \\ &+ \begin{bmatrix} 0 & 0 & \cdots & 0 \\ \boldsymbol{M}_{i[k+1]} & & & \\ & \boldsymbol{M}_{i[k+2]} & & \\ & & \ddots & \\ 0 & \cdots & 0 & \boldsymbol{M}_{i[k+NS]} \end{bmatrix} \begin{bmatrix} \boldsymbol{x}_{a,i[k+1|k]} \\ \boldsymbol{x}_{a,i[k+2|k]} \\ \cdots \\ \boldsymbol{x}_{a,i[k+NS|k]} \end{bmatrix} \\ &+ \begin{bmatrix} \boldsymbol{W}_{[k]} & 0 & \cdots & 0 \\ & \boldsymbol{W}_{[k+1]} & & \\ & & \ddots & \\ & & & \boldsymbol{W}_{[k+NS-1]} \\ 0 & 0 & \cdots & 0 \end{bmatrix} \begin{bmatrix} \Delta u_{i[k|k]} \\ \Delta u_{i[k+1|k]} \\ \cdots \\ \Delta u_{i[k+NS-1|k]} \end{bmatrix} \\ &\leq \begin{bmatrix} \beta_{i[k]} \\ \beta_{i[k+1]} \\ \beta_{i[k+2]} \\ \cdots \\ \beta_{i[k+NS]} \end{bmatrix} \end{aligned} \tag{C4}$$

D. Appendix D

TABLE DI
MAIN PARAMETERS OF FREQUENCY CONTROL MODEL OF TWO-AREA INTERCONNECTED SYSTEM

Parameters	Area1	Area2	Parameters	Area1	Area2
$k_{1,i}$	0.8	0.8	$R_{\mathrm{g},i}$	0.04	0.042
$T_{\mathrm{g},i}$	0.1	0.1	$T_{\mathrm{th},i}$	0.3	0.3
$T_{\mathrm{tr},i}$	8	10	$K_{\mathrm{tr},i}$	0.3	0.3
$k_{2,i}$	0.2	0.2	$R_{\mathrm{w},i}$	0.125	1/24
$T_{\mathrm{wg},i}$	0.2	0.2	$T_{\mathrm{wr},i}$	5	5
$T_{\mathrm{w},i}$	1	1	$R_{\mathrm{wp},i}$	0.05	0.05
$R_{\mathrm{wt},i}$	0.38	0.38	$R_{\mathrm{ge},i}$	1	0.333
a_i	1	0.333	b_i	0.05	0.05
c_i	1	1	X_i	0.6	0.6
Y_i	1	1	$T_{\mathrm{CR},i}$	-0.3	-0.3
$T_{\mathrm{F},i}$	0.23	0.23	$T_{\mathrm{CD},i}$	0.2	0.2
$T_{\mathrm{VFR},i}$	0.05	0.05	$R_{\mathrm{VFR},i}$	1	-0.333
T_{ij}	0.8	0.8	k_{tP}	-0.16	-0.03
k_{tI}	-0.16	-0.03	B_i	20	60
α_i	1	1	D_i	1	3
H_i	6	18			

REFERENCES

[1] P. Makolo, R. Zamora, and T. T. Lie, "The role of inertia for grid flexibility under high penetration of variable renewables-A review of challenges and solutions," *Renewable and Sustainable Energy Reviews*, vol. 147, pp. 111223, Sep. 2021.

[2] Q. H. Wu, Y. Lin, C. Hong, Y. Su, T. Wen and Y. Liu, "Transient stability analysis of large-scale power systems: a survey," *CSEE Journal of Power and Energy Systems*, vol. 9, no. 4, pp. 1284–1300, Jul. 2023,

[3] C. Seneviratne and C. Ozansoy, "Frequency response due to a large generator loss with the increasing penetration of wind/PV generation – A literature review," *Renewable and Sustainable Energy Reviews*, vol. 57, pp. 659–668, May 2016.

[4] X. Tian, Y. Chi, L. Li and H. Liu, "Review of the configuration and transient stability of large-scale renewable energy generation through hybrid DC transmission," *CES Transactions on Electrical Machines and Systems*, vol. 8, no. 2, pp. 115–126, Jun. 2024.

[5] B. Pang, Q. Si, P. Jiang, K. Liao, X. Zhu, J. Yang and Z. He, "Review of the Analysis and Suppression for High-Frequency Oscillations of the Grid-Connected Wind Power Generation System," *CES Transactions on Electrical Machines and Systems*, vol. 8, no. 2, pp. 127–142, Jun. 2024.

[6] X. M. Chen, C. Lu, P. X. Wu, Y. Jiang, H. B. Ye, and X. B. Ling, "Aggregated frequency response model of regional system considering load frequency behaviors," *CSEE Journal of Power and Energy Systems*, to be published.

[7] L. Liu, W. D. Li, Y. Ba, J. K. Shen, C. C. Jin, and K. R. Wen, "An analytical model for frequency nadir prediction following a major disturbance," *IEEE Transactions on Power Systems*, vol. 35, no. 4, pp. 2527–2536, Jul. 2020.

[8] H. Fang and Z. Yu, "Control of virtual synchronous generator for frequency regulation using a coordinated self-adaptive method," *CSEE Journal of Power and Energy Systems*, vol. 10, no. 1, pp. 175–184, Jan. 2024.

[9] I. Alcaide-Godinez, F. Bai, T. K. Saha and R. Memisevic, "Contingency reserve evaluation for fast frequency response of multiple battery energy storage systems in a large-scale power grid," *CSEE Journal of Power and Energy Systems*, vol. 9, no. 3, pp. 873–883, May 2023.

[10] N. N. Ma and D. L. Wang, "Extracting spatial-temporal characteristics of frequency dynamic in large-scale power grids," *IEEE Transactions on Power Systems*, vol. 34, no. 4, pp. 2654–2662, Jul. 2019.

[11] J. K. Shen, W. D. Li, L. Liu, C. C. Jin, K. R. Wen, and X. X. Wang, "Frequency response model and its closed-form solution of two-machine equivalent power system," *IEEE Transactions on Power Systems*, vol. 36, no. 3, pp. 2162–2173, May 2021.

[12] H. Rao, W. Wu, T. Ma, B. R. Zhou, C. Hong, and Y. J. Liu, "Frequency control at the power sending side for HVDC asynchronous interconnections between yunnan power grid and the rest of CSG," *CSEE Journal of Power and Energy Systems*, vol. 7, no. 1, pp. 105–113, Jan. 2021.

[13] W. D. Li, C. C. Jin, K. R. Wen, J. K. Shen, and L. Liu. "Active frequency response control under high-power loss," *Automation of Electric Power Systems*, vol. 42, no. 8, pp. 22–30, Apr. 2018.

[14] C. C. Jin, L. Liu, W. D. Li, X. M. Li, and Y. F. Rao. "A method for the frequency security level grading of power system operation," *Engineering Letters*, vol. 27, no. 3, pp. 623–630, Aug. 2019.

[15] C. C. Jin, W. D. Li, L. Liu, P. Li, and X. Wu, "A coherency identification method of active frequency response control based on support vector clustering for bulk power system," *Energies*, vol. 12, no. 16, pp. 3155, Aug. 2019.

[16] C. C. Jin, W. D. Li, J. K. Shen, P. Li, L. Liu, and K. R. Wen, "Active frequency response based on model predictive control for bulk power system," *IEEE Transactions on Power Systems*, vol. 34, no. 4, pp. 3002–3013, Jul. 2019.

[17] X. Wu, W. D. Li, Z. W. Li, H. C. Zheng, H. Zeng, and Z. F. Li, "Optimal control strategy of active frequency response against large disturbance considering electrochemical energy storage," *Automation of Electric Power Systems*, vol. 47, no. 17, pp. 118–127, Sep. 2023.

[18] X. Wu, W. D. Li, Z. F. Li, C. Zhou, R. B. Wu, and R. B. Ju, "An active frequency response control strategy with security-economy coordination," in *2021 IEEE Sustainable Power and Energy Conference (iSPEC)*, Nanjing, China, 2021, pp. 1511–1516.

[19] T. Baškarad, N. Holjevac, and I. Kuzle. "A new perspective on frequency control in conventional and future interconnected power systems," *In-*

ternational Journal of Electrical Power & Energy Systems, vol. 156, pp. 109731, Feb. 2024.
[20] M. L. Darby and M. Nikolaou. "MPC: Current practice and challenges," *Control Engineering Practice*, vol. 20, no. 4, pp. 328–342, Apr. 2012.
[21] J. F. Hu, Y. H. Shan, J. M. Guerrero, A. Ioinovici, K. W. Chan, and J. Rodriguez, "Model predictive control of microgrids – An overview," *Renewable and Sustainable Energy Reviews*, Vol. 136, pp. 110422, Feb. 2021.
[22] G. L. Tian, Z. C. Du, and Y. J. Li, "Primary frequency regulation for multi-infeed HVDC system using model predictive control and local estimation," *IET Generation, Transmission & Distribution*, vol. 37, no. 20, pp. 4664–4676, Sep. 2023.
[23] A. Varshney, R. Loka, and A. M. Parimi, "Fast frequency response using model predictive control for a hybrid power system," *2021 IEEE 9th International Conference on Smart Energy Grid Engineering (SEGE)*, Oshawa, ON, Canada, 2021, pp. 104–110.
[24] O. Stanojev, U. Markovic, P. Aristidou, G. Hug, D. Callaway, and E. Vrettos, "MPC-based fast frequency control of voltage source converters in low-inertia power systems," *IEEE Transactions on Power Systems*, vol. 37, no. 4, pp. 3209–3220, Jul. 2022.
[25] K. G. Zhang, Z. Li, H. He, M. Wang, Z. B. Zhang, and J. Rodriguez, "Multi-step predictive control based on ant colony optimization for offshore wind turbine system," *2023 IEEE International Conference on Predictive Control of Electrical Drives and Power Electronics (PRECEDE)*, Wuhan, China, 2023, pp. 1–6.
[26] S. Vazquez, J. I. Leon, L. G. Franquelo, J. Rodriguez, H. A. Young, A. Marquez, and P. Zanchetta, "Model predictive control: a review of its applications in power electronics," *IEEE Industrial Electronics Magazine*, vol. 8, no. 1, pp. 16–31, Mar. 2014.
[27] S. H. Li, L. Z. Xiang, and Z. Y. Xiang, "Frequency response enhance control method based on two-step MPC for VSG," *2019 IEEE 3rd Conference on Energy Internet and Energy System Integration (EI2)*, Changsha, China, 2019, pp. 359–363.
[28] J. F. Dai, Y. Tang, Q. Wang, P. Jiang, and Y. Q. Hou, "An extended SFR model with high penetration wind power considering operating regions and wind speed disturbance," *IEEE Access*, vol. 7, pp. 103416–103426, Jul. 2019.
[29] E. F. Camacho and C. Bordons, "Constrained model predictive control," in *Model Predictive Control*, E. F. Camacho and C. Bordons, Eds. London: Springer, 2007, pp. 177–216.
[30] M. Shiroei, A. M. Ranjbar, and T. Amraee, "A functional model predictive control approach for power system load frequency control considering generation rate constraint," *International Transactions on Electrical Energy Systems*, vol. 23, no. 2, pp. 214–229, Mar. 2013.
[31] A. Arab, A. Khodaei, R. Eskandarpour, M. P. Thompson, and Y. Wei, "Three lines of defense for wildfire risk management in electric power grids: a review," *IEEE Access*, vol. 9, pp. 61577–61593, Apr. 2021.

Yan Xie received a B.S. degree in Electrical Engineering and Automation from North China Electric Power University, Baoding, China, in 2012. He received an M.S. degree in Electrical Engineering from North China Electric Power University, Baoding, China, in 2015. He is working toward the Ph.D. degree at China Electric Power Research Institute in Beijing, China. His research interests include power system analysis and control, and dynamic frequency stability control.

Shiying Ma received the B.Sc. degree in Electrical Engineering from Xi'an Jiaotong University, Xi'an, China, in 1990, and the M.Sc. and Ph.D. degrees from China Electric Power Research Institute, Beijing, China, in 1996 and 2013, respectively. He is currently with the Power System Department, and is also a Professor at the Graduate School of China Electric Power Research Institute. He has presided over the development of IEEE standard Guide for Voltage and Reactive Power in 1000 kV and Above AC System and authored or co-authored more than 60 academic papers. His research interests include power system analysis and control, power system simulation technology, and power source-network coordination control technology.

Jiakai Shen received the B.S. degree in Electrical Engineering from North West A&F University, Yangling, China, in 2014. He is currently working toward the Ph.D. degree with the School of Electrical Engineering, Dalian University of Technology, Dalian, China. His research interests include numerical methods for simulation of power system stability and control, and dynamic primary frequency response analysis.

Xiaojun Tang received the B.S. and M.S. degrees in Electrical Engineering and automation from Tianjin University, Tianjin, China, in 2000 and 2004, respectively. He is currently with the Power System Department at Institute of China Electric Power Research Institute. His research interests include power system analysis and control and power source-network coordination control technology.

Jianmiao Ren is working toward the Ph.D. degree at China Electric Power Research Institute, in Beijing, China. His research interests include frequency security-stability control of power systems, and optimal allocation of frequency regulation resources in power systems.

Liwen Zheng received Ph.D degree from the Power System Department at China Electric Power Research Institute, Beijing, China, in 2024. Her research interests include power system stability and control.